Monthly Notices of the ROYAL ASTRONOMICAL SOCIETY
MNRAS **516,** 372–390 (2022) https://doi.org/10.1093/mnras/stac2001

Tailed radio galaxies from the TIFR GMRT sky survey

Netai Bhukta [1], Sushanta K. Mondal [1] and Sabyasachi Pal [2]★
[1]*Department of Physics, Sidho Kanho Birsha University, Ranchi Road, Purulia 723104, India*
[2]*Indian Centre for Space Physics, 43-Chalantika, Garia Station Road, Kolkata 700084, India*

Accepted 2022 July 12. Received 2022 July 11; in original form 2021 October 4

ABSTRACT

We present a list of tailed radio galaxies using the Tata Institute of Fundamental Research (TIFR) Giant Metrewave Radio Telescope (GMRT) Sky Survey Alternative Data Release 1 (TGSS ADR1) at 150 MHz. We visually examined 5336 image fields and found 264 tailed radio galaxies. Tailed radio galaxies are classified as wide-angle tailed (WAT) galaxies or narrow-angle tailed (NAT) galaxies, based on the angle between the two jets of the galaxy. Our sample of tailed radio galaxies included 203 WAT- and 61 NAT-type sources. These newly identified tailed sources are significant additions to the list of known tailed radio galaxies. The source morphology and luminosity features of the various galaxies and their optical identifications are presented. Other radio properties and general features of the sources are also discussed.

Key words: galaxies: active – galaxies: formation – galaxies: jets – galaxies: kinematics and dynamics– radio continuum: galaxies.

1 INTRODUCTION

Tailed radio galaxies are galaxies having a pair of radio 'tails' extending far from the optical galaxy. The radio 'tails' are nothing but the bending of both of the radio jets in the same direction. Initially, they are well collimated on a kiloparsec scale, but then suddenly flare into diffuse plumes, which may be significantly bent (Missaglia et al. 2019; Patra et al. 2019). The spectral index of tailed radio galaxies becomes steeper moving outwards towards the tail from the core and varies from region to region (Bridle et al. 1981; Hardcastle et al. 2003; Patra et al. 2019). Most tailed radio galaxies are Fanaroff–Riley (FR) I radio galaxies (Fanaroff & Riley 1974), for which the surface brightness is higher close to the core than in the regions towards the end of the jets (Terni de Gregory et al. 2017; Missaglia et al. 2019). Tailed radio galaxies are distinguished by their radio morphology, which includes bright hotspots (called 'warmspots') that are closer to their radio core than in FR IIs (Missaglia et al. 2019). Tailed sources are classified depending on the angle between the radio tails and the core of the galaxy. Narrow-angle tail (NAT) radio sources feature tails bent into a narrow 'V' or 'L' shape, where the angle between the two tails is less than 90°. The jet bending in the case of wide-angle tail (WAT) radio sources is such that WATs exhibit wide 'C'-type morphologies, and the angle between the two components is greater than 90° but less than 180°. These 'WAT' and 'NAT' morphologies were first defined by Owen & Rudnick (1976). The structures of NAT sources may be affected by the projection effect. The luminosity of WAT sources is between those of classical double and NAT sources (O'Donoghue, Eilek & Owen 1993).

Tailed sources are generally found in the dynamical, active, and X-ray-intense regions of rich clusters (Burns 1981; O'Dea & Owen 1985). It is considered that the ram pressure associated with the dynamical interaction of the host galaxy with the dense intercluster medium (ICM; assumed to be at rest) causes the radio jets to bend in the reverse direction of motion, away from the cluster centre (Begelman, Rees & Blandford 1979; Vallee, Bridle & Wilson 1981; Baan & McKee 1985). The degree of bending depends on the velocity of the host galaxies (Srivastava & Singhal 2020). NAT sources are found towards the edges of the associated cluster, while WAT sources are generally found close to the gravitational centre of the cluster (Quintana & Lawrie 1982). The ram pressure explanation of jet bending does not hold for WAT sources, as they move very slowly compared with NATs (Burns & Balonek 1982). The WAT morphology is believed to be caused by strong intercluster winds (Burns et al. 1986); in some works, it is attributed to the electromagnetic interaction of the non-neutral jet with the ICM magnetic field (Eilek et al. 1984).

Tailed radio sources can be used to trace galaxy clusters and high-redshift systems (Blanton et al. 2000, 2001; Smolcic et al. 2007); to investigate the inner-cluster environment (Douglas et al. 2011; Wing & Blanton 2011; Blanton et al. 2001); to study the cluster magnetic field (Feretti et al. 1999); to study the interaction of the jet with the ICM; and to study the evolution of galaxies and galactic dynamics (Pinkney et al. 1992). Tailed radio galaxies are normally representatives of FR I sources, but in terms of luminosities, they can be placed close to the FR II transition (Miley et al. 1972; Bliton et al. 1988). On a scale of arcseconds, these tailed galaxies normally have a U-shaped symmetry constructed by a pair of bent jets that originate from the nucleus and meet with the more elongated tails after adequate bending (Owen, Burns & Rudnick 1978; O'Dea & Owen 1986).

A number of factors influence the bending of tailed radio galaxies. (1) Most of the tailed radio galaxy search activities focus on galaxies in clusters (O'Dea & Owen 1985), and the bending of radio tails results from the motion of the host galaxy through the ICM. (2) The hypotheses that host galaxy orbits are radial, circular, or isotropic

★ E-mail: sabya.pal@gmail.com

(Jones & Owen 1979) are tested using the initial ejection angle of the jet with respect to the motion of the galaxy and the jet flow velocity (Baan & McKee 1985). (3) The differences in the ejection of jets with respect to the direction of motion of the host galaxy in the ICM and cluster-environments, as well as projection effects, are responsible for the asymmetries found in the radio jets in some tailed radio galaxies (Sebastian, Lal & Rao 2017). (4) The probability of detection of tailed radio sources decreases in clusters with lower numbers of galaxies (Stocke 1977; Adams, Jensen & Stocke 1980). (5) Various types of bending may be caused by precessing radio jets. Owing to projection effects, the distinction between WATs and NATs is somewhat arbitrary. Many WAT sources look like NAT sources simply as a result of projection effects. Transonic or supersonic relative motions drive the jets of tailed radio galaxies. Even with high-resolution (arcsec-scale) radio observations, a few NAT sources have been discovered to have a remarkable narrow extended structure, with the two radio tails not being resolved (e.g. IC 310; Feretti, Giovannini & Klein 1988).

WATs display less bending of the two jets than NATs, and the bending model of dynamical ram pressure cannot completely explain the bending of WAT morphology (Burns 1981; Burns, Eilek & Owen 1982; Eilek et al. 1984). WAT sources appear to be associated with large-size D or cD galaxies approaching rest at cluster centres (e.g. 3C 465) and therefore should not have the necessary velocity to produce the ram pressure required for the observed bends in their radio jets. So, an alternative fundamental mechanism is required to interpret the observed bending of jets of WATs. An electromagnetic force that results from the interaction of a jet carrying a net electrical current with the magnetic field of the ICM may be responsible for the bending of jets in WATs (Eilek et al. 1984). An ordered magnetic field is required to generate the symmetric shape of WATs. Collisions with dense clouds in the ICM, on the other hand, may also deflect jets. In some WATs, this method may be responsible (Burns et al. 1986), but it is difficult to reproduce the large-scale symmetric structure of WATs by only this method.

O'Dea & Owen (1985) identified 57 tailed sources in the directions of various clusters using the A and B configurations of the Very Large Array (VLA) at 20 cm. This sample of 57 sources includes 41 NATs, 9 WATs and 7 sources with complex morphologies. O'Donghue, Owen & Eilek (1990) identified 11 WATs at 20 cm using the VLA in the A and C configuration. A detailed study of the large WAT 1919 + 479 is presented in Piffaretti et al. (1998). Six other WATs were found in the the Australia Telescope Large Area Survey (ATLAS) field at 1.4 GHz using Australia Telescope Compact Array (Mao et al. 2010). NGC 1265 is a well-studied NAT source (Xu, O'Dea & Biretta 1999). Around 1600 sources have been identified as possible 'tailed' candidates using a pattern-recognition algorithm (Proctor 2016) using the NRAO VLA Sky Survey (NVSS; Condon et al. 1990) at 1.4 GHz.

In this paper, we present 264 tailed radio sources, of which 198 are located in the northern sky (above 0°). We have classified 203 sources as WAT type and 61 sources as NAT type, based on the angle made by the two bent lobes. Most of these sources have been observed before and catalogued in different radio surveys, mostly in the NVSS survey and in the Sydney University Molonglo Sky Survey (SUMSS; Mauch et al. 2003) at 843 MHz, but have not been reported as tailed sources. We found that only about half of the sources are associated with a known galaxy cluster. The optical galaxies hosting the radio sources are located in the redshift range of 0.01 to 0.68, and the total flux at 150 MHz ranges from 0.1 Jy to as high as 20.1 Jy. Redshifts are found for 165 WATs out of 203 detected optical/IR counterparts (75 per cent). For NATs, redshifts are found for 49 galaxies out of 61 detected optical/IR counterparts (76 per cent). Out of 117 identified redshifts of tailed radio galaxies, 50 are identified spectroscopically. The paper is organized as follows. In Section 2, we present the method of the identification of sources. We describe the counterpart identification in Section 3. In the next section (Section 4), we describe the different radio properties of the sources. In Section 5, we discuss the general features and overall properties of sources. We summarize the study in the final section. We assume a flat ΛCDM cosmology with $H_0 = 67.8\,\mathrm{km\,s^{-1}\,Mpc^{-1}}$, $\Omega_\mathrm{M} = 0.308$, and $\Omega_\Lambda = 0.692$ (Aghanim et al. 2020).

2 IDENTIFICATION OF TAILED RADIO GALAXIES

2.1 The TGSS Alternative Data Release 1

Tailed sources are found from the manual inspection of a large number of high-resolution images generated by the Tata Institute of Fundamental Research (TIFR) Giant Metrewave Radio Telescope (GMRT) Sky Survey Alternative Data Release 1 (TGSS ADR 1; Intema et al. 2017). The continuum survey at 150 MHz using the GMRT (Swarup 1991) covers a declination range from −55° to + 90°. The purpose of the survey was to provide a high-resolution and high-sensitivity map of the 150-MHz sky. The median noise of the survey is 3.5 mJy beam^{-1}, and the resolution is 25 arcsec × 25 arcsec north of 19° Dec. and 25 arcsec × 25 arcsec/cos (Dec. − 19°) south of 19°. In total, over 2000 h of observation time were used over about 200 observing sessions. Earlier, four tailed galaxies were serendipitously discovered with GMRT at 610 and 327 MHz (Giacintucci & Venturi 2009). Detection of a WAT (J0037 + 18) with an interacting host galaxy as optical counterpart (Patra et al. 2019) has been reported in the same frequency bands using GMRT.

2.2 Definitions of WATs and NATs

WATs are usually irregular radio galaxies with bright hotspots (also known as 'warmspots' with respect to FR-II) located within host clusters, and their relative rest-frame velocities are low (< 1000 km s^{-1}). Twins of well-collimated radio jets make obtuse bending angles (≥ 90°) under the influence of ICM weather/wind or induced merger shocks. In the 3C catalogue, WAT-3C 465 is known as the prototype (Burns 1981; Eilek et al. 1984; Eilek & Owen 2002; Hardcastle, Sakelliou & Worrall 2005). Because the two tails are bent in the same direction, the implication is probably that the intra-cluster environment should have some regular ICM motion relative to the jets, rather than turbulence motion. We have included a source in our WAT sample if the bending angle is less than 160° and if the source follows the selection criteria given in Subsection 2.3.

NATs are common in clusters, usually moving at high speeds towards the cluster centres (≥ 2000 km s^{-1}; Huchra, Vogeley & Geller 1999; Sun, Jerius & Jones 2005), and their distinctive structures reveal strong interactions with the ICM, with radio tails bent in the same direction as the core of the galaxy.

2.3 Search from TGSS ADR 1

We have made use of the TGSS ADR 1 consisting of images of a total of 5536 fields with a typical noise of ∼5 mJy at 150 MHz. The observations corresponding to this data release were executed between 2010 and early 2012 and cover about 90 per cent of the whole sky. The survey covers 1 steradian of the southern sky, the maximum accessible southern sky from the observatory location. In search of

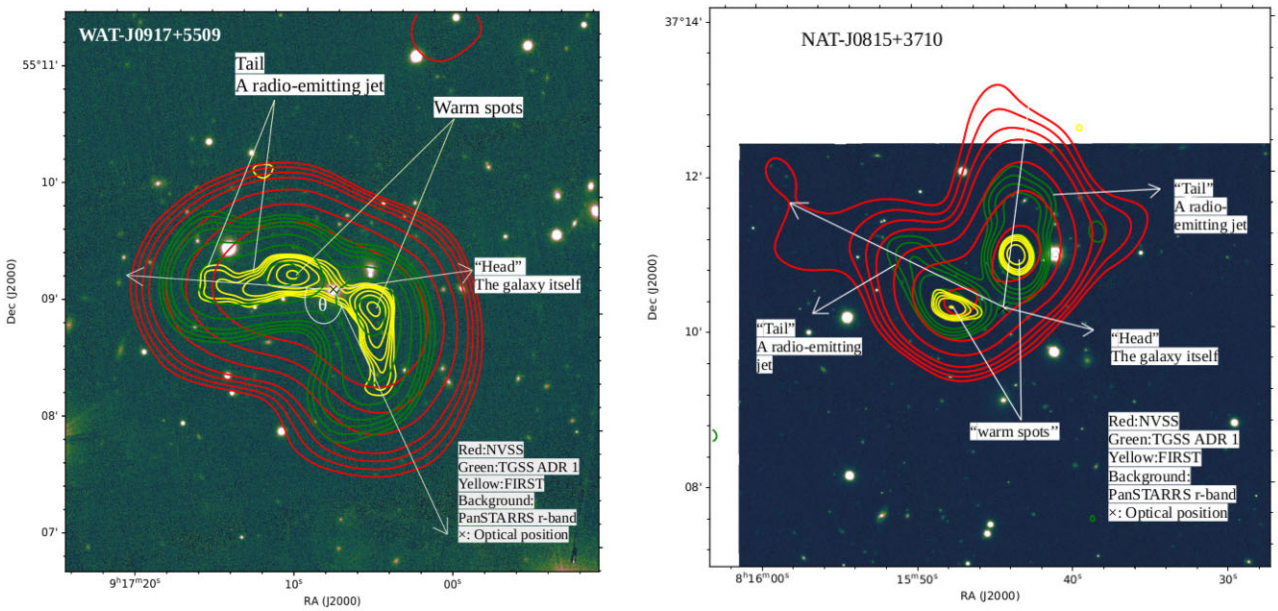

Figure 1. The figure shows an example of ideal WAT (left-hand panel) and NAT (right-hand panel) sources. PanSTARRS *r*-band optical images are overlaid on TGSS, NVSS, and FIRST images. In both of the images, contour levels are at 3σ[–1, 1, 1.4, 2.0, 2.8, 5.6, 11.2, 22.4 mJy beam^{-1}], where σ for the TGSS, FIRST, and NVSS are 3.5, 0.15, and 0.45 mJy beam^{-1}, respectively. Both tailed radio sources are associated with host galaxies or radio cores (known as the 'head'), which are indicated by crosses. A pair of bright hotspots (called 'warmspots') are located closer to their radio core with respect to FR-II. The surface brightness is higher towards the end of the jets than in the regions close to the core. Beyond these warmspots, well-collimated jets suddenly flare into diffuse plumes that may be significantly bent (known as 'tails'). For WATs, the angles (θ) between the two tails of the radio galaxy are $90^\circ \leq \theta \leq 180^\circ$, and for NATs, the angles are $\leq 90^\circ$.

tailed radio galaxies, we closely examined each of these 5536 image fields using Astronomical Imaging Processing Software (AIPS). The good sensitivity and high resolution of TGSS (average rms of 3.5 mJy beam^{-1}) helps in the study of new fainter samples of different types of radio galaxies, such as X-Z-shaped radio galaxies (Bhukta, Pal & Mondal 2022b), and giant radio galaxies (Bhukta, Mondal & Pal 2022a). We visually examined all 5536 fields of TGSS images. For the selection of tailed radio-source samples from TGSS, we opted for the rigorous and tedious method of checking each of the 5536 fields manually. Our source selection criteria are as follows.

1. In order to make an initial list of probable WATs and NATs, we made a list of radio sources showing two-sided jets with a clear bending angle $\leq 160^\circ$.
2. The majority of tailed radio sources show a bright radio centre near the host galaxy, which is known as the 'head'. So, we went through all probable tailed radio sources to check if there was any bright source near the radio-core location. To ensure radio-core positions, we also computed the spectral index near the host galaxy and checked whether the corresponding spectral index was flat. This radio-core position was indicated with a cross.
3. For WAT/NAT sources, radio jets extend into plumes beyond the radio head. We identified sources with warmspots near both sides of the radio head. We measured the peak flux of warmspots of probable WAT/NAT sources, which should be higher than the tail radio flux.
4. We measured the angle between the two tails of all radio sources with the radio core. If the angle of the sources is greater than 90°, then the source is catalogued as a WAT, and if the angle is $\leq 90^\circ$, the source is catalogued as a NAT.
5. All selected sources have a greater angular size than the four times of the synthesized beam .

In Fig. 1, we present the above-mentioned criteria for an ideal radio image of tailed radio sources with surface-brightness contours from TGSS, FIRST, and NVSS radio maps.

We excluded 20 bent sources from our list as they may be radio relics of a cluster. These possible relics were chosen using the following criteria.

1. These diffuse and bent sources are located within 20 kpc of the position of the centre of a known galaxy cluster.
2. There are no optical/IR counterparts or radio cores for these sources. They also lack any warmspots.
3. We studied multiwavelength radio images of these diffuse radio sources.
4. The power-law radio spectrum is steeper ($\alpha \sim 1.2-1.3$).

Similar studies of tailed radio sources have recently been conducted using a variety of methodologies. Double radio sources were found with different morphological radio sources (15 types) via automated pattern recognition using NVSS (Proctor 2011). In this catalogue, 199 C-shaped radio galaxies (either WATs or NATs) were present. From the Proctor sample, Yu-Xing et al. (2019) confirmed 412 C-shaped sources. The sample of detected WATs/NATs is flux-limited and not complete, as the detection depends on the lower contour of each image. It is complete up to 10.2 mJy beam^{-1}.

3 COUNTERPART IDENTIFICATION

This section focuses on the identification of the optical and IR counterparts of the tailed radio sources. We use a likelihood ratio (LR) technique that is particularly useful when dealing with deep optical images to minimize the number of spurious associations. For 261 of our tailed radio sources, we find a reliable counterpart.

3.1 Likelihood ratio technique

The LR technique (Richter 1975; de Ruiter, Willis & Arp 1977; Sutherland & Saunders 1992; Ciliegi, Zamorani & Hasinger 2003) allows us to take into account not only the position of the counterpart but also the background source magnitude distribution and the presence of multiple possible counterparts for a given radio source. It is given by the relationship (Sutherland & Saunders 1992)

$$LR = \frac{q(m) f(r)}{n(m)}, \tag{1}$$

where $n(m)$ represents the surface density of background sources as a function of band magnitude m. This surface density is defined as the ratio of the magnitude distribution of background sources to the total searching area. The parameter $q(m)$ represents the a priori probability that the radio source has a counterpart of magnitude m. According to Ciliegi et al. (2003), the parameter $q(m)$ is derived from

$$q(m) = \frac{real(m) \times Q}{\sum_{m_i} real(m)_i}. \tag{2}$$

The $real(m)$ is calculated from the following equation:

$$real(m) = total(m) - n(m)\, N_{\rm radio}\, \pi r_{\rm max}^2, \tag{3}$$

where $N_{\rm radio}$ is the number of radio sources in the catalogue, $total(m)$ is the total number of objects in the subsidiary catalogue within a radius of $r_{\rm max}(\sim 2$ arcsec) around each radio source, and Q is usually estimated by determining the fraction of sources with radio counterparts above the background as follows:

$$Q = \frac{N_{\rm counterparts} - (\sum_{m_i} n(m)\, r_{\rm max}^2\, N_{\rm radio})}{N_{\rm radio}}. \tag{4}$$

The parameter $f(r)$ represents the probability distribution of the offset r between the catalogued positions of the radio source and its potential counterpart. The uncertainty in this offset is calculated by combining the uncertainty in the radio position, the uncertainty in the optical/IR position, and the uncertainty in the relative astrometry of the two surveys. As for $f(r)$, we adopt a two-dimensional Gaussian distribution of the form

$$f(r) = \frac{1}{2\pi\sigma^2} \exp\left(\frac{-1}{2\sigma^2}\right). \tag{5}$$

For each source, σ is the average value between $\sigma_x = \sqrt{er_{\rm op}^2 + \sigma_\alpha^2}$ and $\sigma_y = \sqrt{er_{\rm op}^2 + \sigma_\delta^2}$, where $er_{\rm op}$ is the position error of the counterpart and σ_α and σ_δ are the radio positional errors in RA and Dec. The LR does not contain information about the possible presence of many counterpart candidates in the surroundings of a specific radio source. It is therefore useful to define the reliability of each association as

$$\rho_j = \frac{(LR)_j}{\sum_i (LR)_i + (1 - Q)}, \tag{6}$$

where the sum is over all the candidate counterparts for the same radio source (Sutherland & Saunders 1992).

3.2 Subsidiary catalogue of WISE and Pan-STARRS data

The selection of multiwavelength data is crucial for identifying the correct counterpart of a radio source. We use two deep optical surveys from the Panoramic Survey Telescope and Rapid Response System (Pan-STARRS; Chambers, Magnier & Metcalfe 2016) and an infrared survey from the Wide-field Infrared Survey Explorer (*WISE*; Wright et al. 2010). Deep and wide optical and IR data are available over the TGSS-ADR 1-covered sky. Pan-STARRS1 has performed a set of independent synoptic imaging sky surveys, including the 3π steradian survey. This survey covers the entire northern sky and the southern sky up to $\delta > -30^\circ$. There are five bands present, namely *grizy* (23.3, 23.2, 23.1, 22.3, 21.4 mag). The typical point spread function (PSF) of the Pan-STARRS images is $\sim$1−1.3 arcsec. In the astrometric calibration, the uncertainty of the standard deviation of the mean and median residuals (Δra, Δdec) are (2.3, 1.7) mas and (3.1, 4.8) mas, respectively. The *WISE* covers a mid-infrared survey of the entire sky. The sensitivity of this survey is much higher than those of previous infrared survey missions. *WISE* achieved a sensitivity more than 100 times better than *IRAS* in the 12-μm band. *WISE* covers the whole sky in four infrared bands, namely W1, W2, W3, and W4 at 3.4, 4.6, 12, and 22 μm, respectively. The All WISE catalogue includes more than 747 million sources across the full sky. The W1 and W2 bands have significantly better sensitivity than the other two WISE bands (Cutri, Strutskie & van Dyk 2013). The completeness of the *WISE* catalogue varies across the sky. With W1 < 19.8, W2 < 19.0, W3 < 16.67, and W4 < 14.32 mag, the completeness is 95 per cent for sources. Initially, we included all WISE sources smaller than 15 arcsec. The *WISE* W1-band and Pan-STARRS *i*-band data sets were combined using LR band magnitude analysis. For each *WISE* source, we searched for the best Pan-STARRS match in the *i* band. LR ratios were then derived for all PanSTARRS sources within 15 arcsec of all WISE positions. And for each *WISE* source, the highest LR above the threshold limit was taken as the PanSTARRS counterpart. Finally, we made a *WISE*–Pan-STARRS combined catalogue that should be used for counterpart identification.

3.3 Cross-match of tailed radio sources with subsidiary catalogues

We used the magnitude and colour in the LR method to cross-match the TGSS ADR1 tailed radio sources with the subsidiary *WISE*–Pan-STARRS combined catalogue. Following the LR method, we built a list of possible counterparts for each of the tailed radio sources. Initially, we set a very low likelihood threshold to be sure not to lose any counterparts. After a careful analysis, we selected only those sources with a reliability greater than 0.6, as the threshold limit to ensure that the expected number of spurious associations is 4 per cent of the subsidiary catalogue. As a result, the number of identified tailed radio sources was maximized. Another approach to measuring a value for the reliability limit, in which those sources with a reliability greater than ρ_c can be accepted as true counterparts, is that of Smith et al. (2011). They estimated the number of false cross-matches using $N_{\rm false} = \sum_{\rho \geq 0.8}(1 - \rho)$ and determined the contamination rate to be $\sim$4.2 (ratio of $N_{\rm false}$ to matched sources with the reliability limit). In our catalogue, $N_{\rm false}$ is 12, and the number of matched sources with the reliability limit is 261. The contamination rate is 4.5 per cent with the reliability limit of 0.6 using the above relationship.

The choice of the best threshold value $LR_{\rm thr}$ is necessary to discriminate between spurious and real identifications. Here, $LR_{\rm thr}$ should be large enough to keep the number of spurious identifications as low as possible and to increase the reliability. We defined a source as counterpart to a tailed radio source if their LRs are above the thresholds of $LR_{\rm thr} = 7.57$ in the *i* band or $LR_{\rm thr} = 0.77$ in the W1 band. If more than one spurious counterpart is above those thresholds, then the counterpart with the highest LR in either of the two bands is accepted and the other is discarded. The counterpart identification rates in our catalogue are 61 per cent and 98 per cent in the *i* and W1 bands, respectively. We also calculated the radio optical separation of

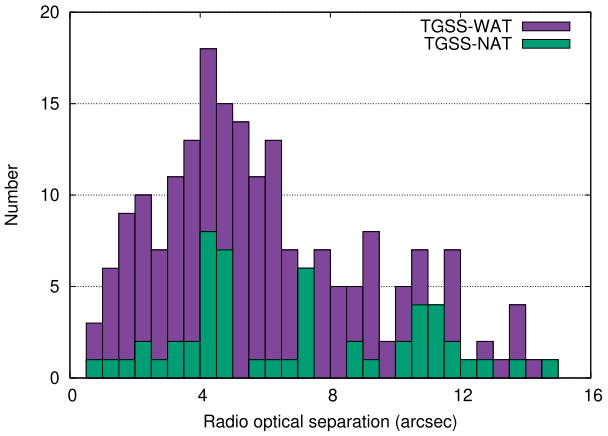

Figure 2. Distribution representing the separation between radio and optical positions of tailed radio sources.

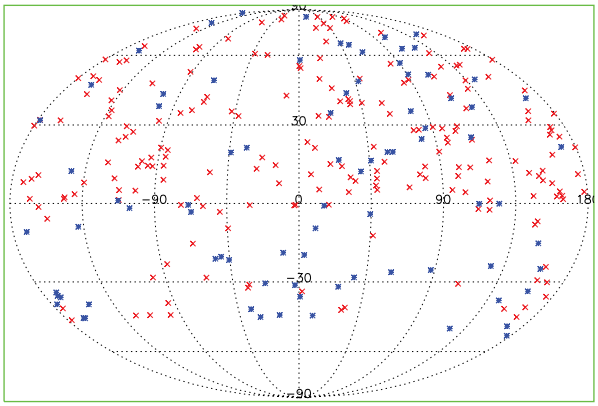

Figure 3. The spatial distribution of tailed radio sources. The red crosses indicate WAT sources, and the blue asterisks represent NAT sources.

each radio source with the highest reliability. The separation between the radio and optical position is shown in Tables 1 and 2. With this criteria, a 3 per cent counterpart (8/261) is identified with spurious association. Fig. 2 presents the distribution of the separation between optical and radio counterparts. A peak is seen near 4 arcsec.

We made use of other previous all-sky surveys. In particular, we used the SDSS DR-12 catalogue (Alam et al. 2015), the Two Micron All Sky Survey (2MASS; Skrutskie et al. 2006), and the extended source catalogue (2MASX; Jarrett, Chester & Cutri 2000). We found optical counterparts for 57 WATs in SDSS, for 26 in the 2MASS catalogue, and for 13 in the 2MASX catalogue. We also identified optical counterparts for 10 NATs in SDSS, for 11 in the 2MASS catalogue, and for 17 in the 2MASX catalogue. In our catalogue, about 117 tailed radio galaxies (92 WATs and 25 NATs) have redshift information. For 92 WATs, spectroscopic redshift data can be collected from the SDSS for 34, and for NATs, for three. Because optical/IR counterparts are more compact than the corresponding radio galaxies, we used the positions of optical/IR counterparts as the positions of these sources. For the remaining four (1 per cent of the total detected sources) tailed radio sources, where optical or IR counterparts are not available, a radio-morphology-based position was used.

From a visual search, Dehghan et al. (2014) detected 56 bent tailed radio sources over an area of ∼4 square degrees of the southern sky in the ATLAS field. From combined mosaic radio sources (FR-I and FR-II) of the southern sky, 24 new bent-tailed samples were identified by visual inspection (O'Brien et al. 2018). Missaglia et al. (2019) presented a catalogue of 47 WATs. All candidates were selected by combining observations from the NVSS, FIRST, and SDSS surveys. With the help of the VLA FIRST survey at 1.4 GHz, Sasmal et al. (2022) found 717 new head–tail radio galaxies; among them, 430 were WATs and 287 were NATs. Pal & Kumari (2022) presented a catalogue of 50 new head–tail radio sources (5 NATs and 45 WATs) using the LOFAR Two-metre Sky Survey first data release (LoTSS DR1) at 144-MHz frequency (Shimwell et al. 2019). The survey coverage area of the present paper is larger than in all other previous works.

4 RESULTS

Information about the objects reported in this paper is given in Tables 1 and 2. In the first two columns, the catalogue number and identification names are given. Columns (3) and (4) contain the J2000 coordinates of the optical/IR counterpart. The radio counterpart separation is presented in column (5). For cases where the optical counterpart is not found, the approximate position using the morphology of the radio source is provided. The reliability of the counterpart (ρ) is presented in columns (6). In columns (7) and (8), the total flux densities in Jy at 150 MHz (F_{150}) and 1400 MHz (F_{1400}) obtained from the TGSS and NVSS surveys are provided. Columns (9) and (10) contain the spectral index and redshift of the sources, respectively. In column (11), we provide the luminosity at 150 MHz. Column (12) contains the names of earlier radio surveys in which the source is presented without identification of them as tailed radio galaxies.

We report the discovery of 203 WAT and 61 NAT sources from the TGSS ADR 1 at 150 MHz. We removed sources reported in Proctor (2011) and other catalogues from our list (Dehghan et al. 2014; Missaglia et al. 2019; Yu-Xing et al. 2019). Dehghan et al. (2014) identified 45 bent-tailed (BT) radio galaxies in the Australia Telescope Large Area Survey (ATLAS) at 1.4 GHz, which is supplemented with the 1.4-GHz Very Large Array images. Proctor (2011) identified 199 WAT or NAT radio galaxies using an automated morphological classification scheme. Missaglia et al. (2019) presented a catalogue of 47 WAT radio galaxies. All candidates were selected by combining observations of the NVSS survey, FIRST survey, and SDSS survey. We present the spatial distribution of the newly identified WAT and NAT sources in Fig. 3. As expected, the sources show a random distribution. Many of these newly identified sources are catalogued as two separate sources in the NVSS catalogue (Condon et al. 1990). The number of sources is higher in the northern region than in the southern region because the survey is limited up to a declination of –55° and the local RMS in the Southern hemisphere is higher that of the Northern hemisphere owing to high-declination effects.

We present high-sensitivity 150-MHz GMRT images of ideal selected WAT and NAT radio galaxies in Fig. 1, as identified from the TGSS as examples of WAT and NAT sources discovered under the present project. We present the radio images of tailed radio sources with different contours from TGSS ADR 1, NVSS, and FIRST. PanSTARRS r-band optical images are overlaid with TGSS, NVSS, and FIRST images. In all figures, contour levels are at 3σ[–1, 1, 1.4, 2.0, 2.8, 5.6, 11.2, 22.4 mJy beam^{-1}], and σ for the TGSS, FIRST, and NVSS is 3.5, 0.15, and 0.45 mJy beam^{-1}, respectively. Overlaid images of all the tailed radio sources are available as supporting information in the online version of the article.

4.1 Spectral index

The two-point spectral index of newly discovered radio galaxies between 150 and 1400 MHz is calculated assuming $F \propto \nu^{-\alpha}$, where

Table 1. Candidate WAT radio sources.

Cat. no.	Name	RA core (J2000.0)	Dec. core (J2000.0)	Separation (arcsec)	ρ	F_{150} (Jy)	F_{1400} (Jy)	$\alpha_{0.15}^{1.4}$ ($\pm$0.05)	z	L_{150} WHz^{-1} $\times 10^{25}$	Other catalogue
(1)	(2)	(3)	(4)	(5)	(6)	(7)	(8)	(9)	(10)	(11)	(12)
1	J0001 + 5458	00 01 21.8	+ 54 58 10	5.20	0.90	0.59	0.10	0.79	–	–	1, 8
2	J0003 – 3556	00 03 11.5	– 35 56 38	2.12	0.99	7.16	–	–	0.05	–	14
3	J0005 + 5359	00 05 46.3	+ 53 59 57	3.50	0.99	0.67	0.09	0.89	–	–	1, 8
4	J0008 – 3347	00 08 49.6	– 33 47 51	6.03	0.89	0.33	0.03	1.07	–	–	1, 14
5	J0022 + 2317	00 22 24.4	+ 23 17 25	5.14	0.99	2.14	0.41	0.73	0.13	9.36	1
6	J0041 + 2104	00 41 43.1	+ 21 04 26	5.01	0.99	0.35	0.33	0.02	–	–	1
7	J0050 + 0514	00 50 44.6	+ 05 15 01	3.12	0.99	0.27	0.10	0.44	0.27[b]	5.42	1
8	J0054 + 3339	00 54 43.8	+ 33 39 01	6.58	0.99	0.33	0.06	0.76	–	–	1, 4
9	J0104 + 8210	01 04 25.1	+ 82 10 31	6.47	0.89	0.66	0.19	0.55	–	–	1, 4
10	J0106 + 4909	01 06 48.6	+ 49 08 56	9.28	0.99	0.43	0.07	0.81	–	–	1
11	J0114 + 0029	01 14 25.6	+ 00 29 33	6.69	0.99	0.36	0.09	0.62	0.35	13.46	11
12	J0119 + 5838	01 19 35.3	+ 58 38 54	4.71	0.99	0.55	0.08	0.86	–	–	1, 8
13	J0120 + 1451	01 20 01.1	+ 14 51 38	6.29	0.88	0.59	0.16	0.58	0.05[b]	0.34	1, 8
14	J0123 + 3315	01 23 39.9	+ 33 15 22	0.29	0.99	1.43	0.10	1.19	0.02	0.12	1
15	J0128 + 3448	01 28 59.1	+ 34 48 42	6.18	0.99	0.73	0.14	0.73	0.15	4.32	1,4
16	J0139 + 7444	01 39 25.2	+ 74 44 58	2.31	0.99	0.15	0.04	0.59	–	–	1, 8
17	J0141 + 4506	01 41 37.0	+ 45 06 07	2.10	0.99	0.31	0.09	0.55	–	–	1
18	J0149 + 1403	01 49 11.9	+ 14 03 01	6.22	0.99	0.46	0.13	0.56	0.07	0.53	1
19	J0200 + 3935	02 00 53.0	+ 39 35 01	6.46	0.99	1.80	0.61	0.48	–	–	10
20	J0203 + 6702	02 03 08.5	+ 67 02 52	1.95	0.99	0.89	0.12	0.89	–	–	1, 4
21	J0204 + 0415	02 04 28.9	+ 04 15 17	4.95	0.99	0.33	0.10	0.53	0.14[a]	1.64	11
22	J0205 – 4124	02 05 40.4	– 41 24 13	6.08	0.99	1.10	–	–	–	–	–
23	J0209 + 0950	02 09 47.6	+ 09 50 02	3.68	0.96	4.69	1.25	0.59	–	–	1
24	J0225 + 4031	02 25 44.9	+ 40 31 33	1.49	0.95	3.93	0.91	0.65	0.14	199.09	3
25	J0228 + 3821	02 28 30.3	+ 38 21 12	7.77	0.99	1.07	0.22	0.70	0.03	0.21	4, 10
26	J0229 + 3942	02 29 47.8	+ 39 42 29	1.34	0.99	0.98	0.15	0.84	–	–	4, 10
27	J0245 + 8207	02 45 20.2	+ 82 07 15	1.61	0.99	1.38	0.18	0.91	–	–	1
28	J0257 – 0400	02 57 43.8	– 03 59 59	3.61	0.99	1.10	–	–	0.18[b]	–	6, 11
29	J0300 + 7438	03 00 32.1	+ 74 38 59	–	–	2.36	0.32	0.89	–	–	1, 2
30	J0303 + 3856	03 03 0.44	+ 38 56 39	9.98	0.98	0.95	0.18	0.74	0.28[a]	22.28	1,4
31	J0306 – 1206	03 06 58.6	– 12 06 43	3.31	0.99	5.94	1.39	0.65	–	–	1, 2
32	J0310 + 4803	03 10 16.9	+ 48 03 27	2.17	0.99	2.07	0.55	0.59	–	–	1, 3
33	J0312 + 0644	03 12 51.7	+ 06 44 48	7.42	0.99	0.41	0.06	0.86	–	–	1
34	J0315 + 0507	03 15 30.6	+ 05 07 46	5.30	0.99	0.38	0.10	0.59	–	–	1
35	J0316 + 0922	03 15 59.9	+ 09 23 01	3.89	0.82	0.45	0.13	0.55	–	–	6
36	J0317 + 4917	03 17 33.3	+ 49 17 19	4.43	0.89	1.56	0.40	0.60	–	–	1, 8
37	J0338 + 1544	03 38 04.5	+ 15 44 19	11.7	0.93	0.16	0.08	0.31	0.03[b]	18.92	1
38	J0348 + 1924	03 48 28.4	+ 19 24 19	10.1	0.98	1.23	0.23	0.75	–	–	1
39	J0401 + 3853	04 01 4.30	+ 38 53 00	4.15	0.65	0.55	0.13	0.64	–	–	1, 10
40	J0402 + 1929	04 02 13.0	+ 19 29 07	8.54	0.64	2.58	0.78	0.53	–	–	1
41	J0405 – 2610	04 05 15.9	– 26 10 58	1.23	0.99	0.93	0.18	0.73	–	–	1
42	J0415 + 3428	04 15 13.5	+ 34 28 29	3.23	0.99	0.68	0.14	0.70	–	–	1, 4, 8
43	J0436 + 0603	04 36 22.5	+ 06 03 12	7.63	0.99	1.45	0.24	0.70	–	–	1
44	J0458 + 8206	04 58 38.3	+ 82 06 35	4.50	0.99	0.51	0.08	0.82	–	–	2, 4
45	J0505 + 1056	05 05 08.1	+ 10 56 08	2.11	0.99	1.34	0.28	0.70	–	–	1
46	J0508 + 2754	05 08 12.3	+ 27 54 15	4.64	0.87	2.36	0.40	0.79	–	–	1
47	J0520 + 1356	05 20 12.5	+ 13 56 01	4.77	0.99	0.95	0.22	0.65	–	–	1, 3
48	J0522 + 2807	05 22 46.0	+ 28 06 40	6.65	0.99	1.91	–	–	–	–	–
49	J0528 + 5601	05 28 38.3	+ 56 01 49	1.33	0.99	0.43	0.07	0.81	–	–	4
50	J0533 + 4727	05 33 54.8	+ 47 27 07	10.5	0.82	2.49	0.34	1.12	–	–	1, 4, 10
51	J0542 + 7902	05 42 58.0	+ 79 02 31	–	–	0.61	0.16	0.59	–	–	15
52	J0602 + 1937	06 02 37.2	+ 19 37 05	4.57	0.99	0.85	0.14	0.80	–	–	1, 8
53	J0602 + 2911	06 02 34.1	+ 29 11 06	9.66	0.82	2.99	0.48	0.81	–	–	1, 2
54	J0608 + 8058	06 08 32.1	+ 80 58 12	1.52	0.99	0.77	0.16	0.70	–	–	1, 4
55	J0623 + 0504	06 23 11.5	+ 05 04 12	4.29	0.99	0.85	0.15	0.77	–	–	1, 6
56	J0626 + 2838	06 26 38.6	+ 28 38 42	2.16	0.99	0.72	0.09	0.93	–	–	1, 8, 9
57	J0630 + 2306	06 30 31.4	+ 23 06 05	6.02	0.99	0.52	0.09	0.78	–	–	16
58	J0631 + 2500	06 31 25.8	+ 25 00 48	1.94	0.99	13.3	1.08	1.12	0.08[a]	3.39	1
59	J0640 + 1020	06 40 41.6	+ 10 20 36	6.20	0.95	0.56	0.12	0.68	–	–	1,15
60	J0645 + 1340	06 45 28.0	+ 13 40 25	–	–	1.01	0.13	0.91	–	–	1, 2
61	J0653 + 6919	06 53 17.8	+ 69 19 39	4.41	0.99	8.18	1.38	0.79	–	–	1, 2, 4

Table 1 – *continued*

Cat. no.	Name	RA core (J2000.0)	Dec. core (J2000.0)	Separation (arcsec)	ρ	F_{150} (Jy)	F_{1400} (Jy)	$\alpha_{0.15}^{1.4}$ ($\pm$0.05)	z	L_{150} WHz^{-1} $\times 10^{25}$	Other catalogue
(1)	(2)	(3)	(4)	(5)	(6)	(7)	(8)	(9)	(10)	(11)	(12)
62	J0655 + 0412	06 55 20.3	+ 04 12 09	3.14	0.99	2.49	0.30	0.94	–	–	6
63	J0700 + 2736	07 00 01.0	+ 27 36 28	5.94	0.99	1.73	0.31	0.76	–	–	1,9
64	J0708 + 2928	07 08 48.5	+ 29 28 13	5.24	0.99	1.22	0.16	0.90	0.19	12.44	1,9
65	J0714 + 1334	07 14 10.5	+ 13 34 49	6.33	0.99	0.45	0.10	0.67	0.54	46.12	1, 8
66	J0715 – 3044	07 15 24.8	– 30 43 45	10.1	0.96	1.65	0.30	0.76	–	–	1
67	J0724 + 5010	07 24 31.5	+ 50 10 53	3.96	0.61	1.00	0.15	0.84	–	–	1, 8, 11
68	J0736 + 2412	07 36 21.8	+ 24 12 14	5.29	0.99	4.88	0.44	1.07	0.15	30.35	1, 2
69	J0752 + 0814	07 52 57.0	+ 08 14 33	7.20	0.93	0.64	0.04	1.24	–	–	1, 2
70	J0756 + 0107	07 56 7.31	+ 01 07 48	4.37	0.76	1.30	0.41	0.51	–	–	1
71	J0757 + 3640	07 57 53.2	+ 36 40 22	6.91	0.99	1.44	0.32	0.67	0.12[a]	5.25	12, 13
72	J0805 + 1614	08 05 44.8	+ 16 14 05	2.46	0.99	1.01	0.18	0.77	0.10[b]	2.48	12
73	J0818 + 5437	08 18 06.6	+ 54 37 32	3.18	0.99	3.31	0.51	0.83	0.12[b]	12.28	11
74	J0831 + 6104	08 31 48.8	+ 61 04 59	9.36	0.98	1.24	0.14	0.97	–	–	1
75	J0841 + 4451	08 41 04.3	+ 44 51 04	1.86	0.65	0.48	0.07	0.86	0.27	10.67	1, 10, 11
76	J0856 + 4829	08 56 1.17	+ 48 29 20	10.2	0.99	0.44	0.16	0.45	0.12[b]	0.15	4, 8, 11
77	J0912 + 1600	09 12 35.2	+ 16 00 01	7.33	0.99	0.10	0.02	0.72	0.08[b]	1.55	1
78	J0917 + 5509	09 17 08.0	+ 55 09 08	4.34	0.99	1.30	0.22	0.79	0.19	13.13	4,8
79	J0932 + 5533	09 32 01.0	+ 55 33 47	0.80	0.99	0.81	0.17	0.69	0.26[b]	15.92	1, 11
80	J0940 + 1131	09 40 34.4	+ 11 31 40	3.94	0.99	2.76	0.58	0.69	0.08[b]	1.32	1
81	J0944 + 0247	09 44 43.4	+ 02 47 57	2.96	0.68	3.73	0.35	1.05	0.22	3.64	1,6
82	J0951 – 0757	09 51 30.2	– 07 57 51	3.81	0.99	0.72	–		–	–	–
83	J0957 – 0644	09 57 00.4	– 06 44 26	8.44	0.99	2.27	0.40	0.77	0.13	9.96	1,6
84	J1003 + 1019	10 03 41.9	+ 10 20 01	5.33	0.99	0.69	0.20	0.55	0.18	0.89	1, 11, 16
85	J1008 – 4055	10 08 11.0	– 40 55 44	9.12	0.99	0.66	–	–	–	–	14
86	J1009 – 1504	10 09 07.3	– 15 04 04	1.67	0.92	1.96	0.12	1.25	–	–	1, 2
87	J1012 + 0841	10 12 06.4	+ 08 41 33	5.88	0.99	0.87	0.21	0.63	0.09	1.72	1,11
88	J1015 + 1221	10 15 41.1	+ 12 21 01	7.41	0.99	0.35	0.10	0.56	–	–	1, 11
89	J1019 + 7020	10 19 56.1	+ 70 20 22	5.42	0.99	0.72	0.12	0.80	–	–	1, 4, 8
90	J1022 + 5006	10 22 28.4	+ 50 06 20	4.24	0.65	0.73	0.03	1.42	0.16	5.51	2,4
91	J1032 + 3151	10 32 18.0	+ 31 51 42	3.60	0.99	0.79	0.16	0.71	0.35	30.40	1, 9, 11
92	J1034 + 0736	10 34 10.0	+ 07 36 05	3.76	0.97	0.92	0.12	0.91	0.58[b]	123.92	1, 2, 11
93	J1038 – 3346	10 38 47.9	– 33 46 35	3.97	0.99	0.50	0.06	0.94	–	–	1
94	J1042 + 0237	10 42 31.3	+ 02 37 10	8.65	0.99	0.87	0.12	0.88	0.18[b]	7.85	1, 6, 11
95	J1046 – 2911	10 46 09.9	– 29 21 10	3.48	0.99	2.14	0.55	0.60	0.06	1.81	1
96	J1048 + 3532	10 48 49.0	+ 35 32 01	3.51	0.99	1.94	0.22	0.97	0.39	104.11	1, 4, 13
97	J1050 + 0432	10 50 57.6	+ 04 32 17	10.2	0.99	0.34	0.08	0.64	0.12	1.23	1
98	J1050 – 2405	10 50 34.5	– 24 05 57	5.95	0.99	3.19	0.67	0.69	0.03	0.63	1
99	J1051 + 1825	10 51 57.7	+ 18 25 38	5.61	0.99	0.49	0.11	0.66	0.55[b]	1.48	1, 11
100	J1056 + 0255	10 56 17.0	+ 02 55 26	1.94	0.97	0.54	0.07	0.91	0.39	28.40	1
101	J1058 + 0136	10 58 07.5	+ 01 36 19	2.34	0.99	1.26	0.04	1.54	0.04	0.47	1, 2
102	J1106 – 4018	11 06 58.0	– 40 18 55	10.5	0.93	0.65	–	–	–	–	14
103	J1108 – 4424	11 08 11.0	– 44 24 30	1.68	0.62	0.55	–	–	–	–	14
104	J1108 + 2610	11 08 12.5	+ 26 10 34	5.96	0.95	0.66	0.12	0.76	0.17[b]	5.16	11, 13
105	J1116 – 3010	11 16 00.1	– 30 10 08	1.95	0.99	0.73	0.12	0.80	–	–	1
106	J1118 + 2754	11 18 59.4	+ 27 54 07	7.10	0.99	2.05	0.52	0.61	0.06	1.74	11
107	J1119 + 6317	11 19 33.2	+ 63 17 17	4.39	0.99	0.42	0.11	0.59	0.16	2.80	1,4,11
108	J1120 + 2912	11 20 38.5	+ 29 12 34	5.26	0.99	0.28	0.08	0.56	0.24[b]	4.48	1, 11
109	J1130 + 2524	11 30 48.8	+ 25 24 36	2.99	0.99	0.41	0.09	0.67	0.14[b]	2.08	1, 11
110	J1131 + 4408	11 31 10.1	+ 44 08 15	10.1	0.85	0.49	0.06	0.94	–	–	1, 2, 10
111	J1132 + 6311	11 32 51.0	+ 63 11 44	3.59	0.99	1.90	0.43	0.66	0.11[b]	1.30	1, 4
112	J1141 – 3357	11 41 28.9	– 35 57 10	5.45	0.99	0.32	–	–	–	–	1
113	J1142 + 1102	11 42 54.3	+ 11 01 33	8.53	0.99	1.30	0.34	0.60	0.15[b]	7.57	17
114	J1151 + 0422	11 51 46.9	+ 04 22 23	2.73	0.86	0.39	0.09	0.65	0.13	1.68	1,11
115	J1155 + 5755	11 55 58.3	+ 57 55 27	9.30	0.93	0.38	0.11	0.55	–	–	2, 11
116	J1156 + 3432	11 56 7.40	+ 34 32 47	5.32	0.98	1.03	0.15	0.86	–	–	1, 11, 13
117	J1158 + 2117	11 58 37.2	+ 21 17 11	5.98	0.99	0.36	0.07	0.73	–	–	1,11
118	J1200 + 2942	12 00 46.1	+ 29 42 58	7.52	0.99	1.20	0.24	0.72	0.16	8.18	11, 13
119	J1202 + 5802	12 02 3.80	+ 58 02 08	3.59	0.99	5.70	0.85	0.85	0.10[b]	14.42	1, 11
120	J1205 + 3204	12 05 14.5	+ 32 04 17	5.03	0.99	0.72	0.18	0.62	0.16	4.83	11,13
121	J1206 + 3152	12 06 47.6	+ 31 52 31	1.59	0.89	0.80	0.17	0.69	0.25	14.48	11,13

Table 1 – *continued*

Cat. no.	Name	RA core (J2000.0)	Dec. core (J2000.0)	Separation (arcsec)	ρ	F_{150} (Jy)	F_{1400} (Jy)	$\alpha_{0.15}^{1.4}$ ($\pm$0.05)	z	L_{150} WHz^{-1} $\times 10^{25}$	Other catalogue
(1)	(2)	(3)	(4)	(5)	(6)	(7)	(8)	(9)	(10)	(11)	(12)
122	J1212 – 4545	12 12 20.7	– 45 45 20	1.99	0.99	1.96	–	–	0.16	–	6
123	J1221 – 4046	12 21 24.4	– 40 46 15	0.96	0.98	0.32	–	–	–	–	14
124	J1234 – 1045	12 34 29.6	– 10 45 25	7.78	0.95	0.34	0.06	0.77	–	–	1
125	J1242 – 3613	12 42 01.0	– 36 13 40	2.28	0.68	1.52	0.28	0.75	–	–	1
126	J1242 + 5021	12 42 7.40	+ 50 21 47	1.50	0.99	0.34	0.10	0.54	0.15	1.96	1,8
127	J1249 + 0144	12 49 42.9	+ 01 44 18	3.79	0.94	0.50	0.20	0.41	–	–	1
128	J1304 + 1041	13 04 17.9	+ 10 40 35	2.53	0.99	0.44	0.05	0.97	0.11[b]	1.12	1
129	J1304 + 6439	13 04 28.8	+ 64 39 38	4.48	0.88	1.83	0.31	0.79	0.23[b]	27.98	1, 4, 8
130	J1307 + 5651	13 07 43.7	+ 56 51 03	2.23	0.99	0.72	0.13	0.76	0.24	8.78	4,8,11
131	J1311 – 0120	13 11 31.7	– 01 20 00	4.88	0.99	1.09	0.05	1.37	0.18	10.68	1
132	J1315 + 4841	13 15 30.5	+ 48 41 14	7.67	0.86	0.45	0.07	0.83	0.68[b]	85.27	1
133	J1325 + 5736	13 25 11.2	+ 57 36 01	3.98	0.99	1.63	0.10	1.24	0.12[b]	5.24	1
134	J1331 – 0544	13 31 24.3	– 05 44 36	4.05	0.99	2.92	0.67	0.66	0.15	5.88	1
135	J1412 + 7420	14 12 25.8	+ 74 20 19	1.40	0.99	1.23	0.21	0.79	0.21	13.80	1
136	J1414 + 0143	14 14 32.6	+ 01 43 54	6.12	0.99	0.56	0.19	0.48	0.05[b]	0.32	1
137	J1416 + 0219	14 16 13.4	+ 02 19 08	6.46	0.99	0.70	0.25	0.46	0.16[b]	3.94	1
138	J1440 + 0328	14 40 39.0	+ 03 28 37	3.94	0.99	0.61	–	–	0.03	–	2
139	J1449 + 3959	14 49 0.86	+ 40 00 44	2.09	0.99	1.68	0.26	0.83	–	–	1, 11, 13
140	J1450 + 4418	14 50 39.8	+ 44 18 29	3.10	0.99	1.45	0.28	0.73	0.29[b]	33.94	1, 13
141	J1501 + 0752	15 01 57.4	+ 07 52 27	10.2	0.97	2.55	0.50	0.72	0.66[b]	362.4	1, 11
142	J1508 + 3554	15 08 34.1	+ 35 54 28	9.36	0.68	0.90	0.18	0.72	0.12[b]	3.68	4, 9
143	J1509 + 3327	15 09 59.7	+ 33 27 46	9.84	0.99	0.85	0.17	0.72	0.12[b]	3.12	1, 13
144	J1543 – 4345	15 43 13.5	– 43 45 01	5.55	0.99	3.39	–	–	–	–	–
145	J1553 + 1530	15 53 45.5	+ 15 30 14	3.00	0.98	0.72	0.14	0.73	0.13[b]	3.14	1, 8, 11
146	J1604 + 2355	16 04 56.7	+ 23 55 58	3.13	0.99	4.13	0.66	0.82	0.03	2.70	1, 13
147	J1612 + 2929	16 12 35.4	+ 29 29 05	3.85	0.99	0.55	0.11	0.72	0.03	1.78	1, 13
148	J1615 + 4711	16 15 44.1	+ 47 11 45	9.56	0.99	4.88	0.57	0.96	–	–	1, 4, 11
149	J1616 + 0926	16 16 53.2	+ 09 26 36	7.84	0.89	4.88	0.23	1.36	0.20	60.75	1
150	J1620 + 2521	16 20 35.8	+ 25 21 04	1.23	0.99	0.62	0.18	0.55	–	–	1, 13
151	J1627 – 4336	16 27 01.0	– 43 36 20	7.82	0.99	2.35	–	–	–	–	6
152	J1631 + 0115	16 31 30.4	+ 01 16 14	2.81	0.95	0.43	0.06	0.88	–	–	1
153	J1631 + 0501	16 31 06.1	+ 05 01 27	8.74	0.84	1.19	0.17	0.86	–	–	1
154	J1636 + 2718	16 36 5.20	+ 27 18 35	4.28	0.99	1.78	0.43	0.63	0.13[b]	7.76	1, 9, 11
155	J1658 + 6256	16 58 47.1	+ 62 56 25	3.79	0.99	1.31	0.29	0.67	0.10[b]	3.24	1, 4, 8
156	J1701 + 6413	17 01 32.0	+ 64 13 38	6.11	0.99	0.37	0.07	0.74	–	–	1, 4, 8
157	J1711 + 0449	17 11 53.0	+ 04 49 28	8.22	0.99	1.37	0.16	0.96	–	–	1, 8
158	J1711 + 1351	17 11 50.9	+ 13 51 51	5.82	0.99	0.44	0.24	0.27	–	–	1
159	J1717 + 3734	17 17 25.4	+ 37 34 59	5.14	0.99	0.37	0.15	0.40	0.09	0.71	1,13
160	J1719 + 1557	17 19 39.6	+ 15 57 40	1.08	0.99	3.60	0.08	1.70	–	–	1
161	J1727 – 2815	17 27 01.1	– 28 15 30	1.04	0.99	2.34	0.06	1.64	–	–	1, 15
162	J1729 – 4330	17 29 56.8	– 43 30 55	2.61	0.99	0.76	0.19	0.62	–	–	1, 6
163	J1735 + 3137	17 35 06.5	+ 31 37 51	9.00	0.99	0.56	0.12	0.69	0.28	2.03	1, 9
164	J1736 + 1414	17 36 19.4	+ 14 14 58	1.59	0.52	0.46	0.07	0.84	–	–	1
165	J1741 – 3831	17 41 01.0	– 38 32 05	3.65	0.99	0.76	0.19	0.62	–	–	1, 6
166	J1741 + 1720	17 41 39.2	+ 17 20 34	9.43	0.99	9.05	1.58	0.78	0.06	7.78	1
167	J1748 + 1400	17 48 26.2	+ 14 00 54	7.16	0.82	1.14	0.11	1.04	–	–	1, 2
168	J1752 + 5218	17 52 52.6	+ 52 17 56	6.35	0.99	0.19	0.03	0.82	–	–	1
169	J1801 + 2109	18 01 48.5	+ 21 09 27	7.23	0.86	4.48	0.84	0.75	–	–	1
170	J1814 – 2302	18 14 39.5	– 23 02 38	10.5	0.99	1.73	0.09	1.32	–	–	1
171	J1816 + 1415	18 16 29.2	+ 14 15 09	8.54	0.99	3.28	0.60	0.76	–	–	1, 2
172	J1818 + 1739	18 18 08.5	+ 17 39 42	10.5	0.98	0.99	0.10	1.02	–	–	1
173	J1820 + 0855	18 20 2.20	+ 08 55 14	8.40	0.72	1.87	0.25	0.90	–	–	15, 16
174	J1820 + 2011	18 20 25.5	+ 20 11 55	0.53	0.99	0.37	0.07	0.74	–	–	1
175	J1826 + 3449	18 26 50.2	+ 34 49 40	2.54	0.93	3.72	0.12	1.53	–	–	1, 9
176	J1827 + 6832	18 27 31.8	+ 68 32 15	3.47	0.99	0.76	0.15	0.72	–	–	1, 5
177	J1856 + 3556	18 56 24.3	+ 35 56 18	5.96	0.98	1.87	0.57	0.53	–	–	1, 2, 9
178	J1906 – 0033	19 06 16.0	– 00 33 29	3.82	0.99	0.92	0.18	0.73	–	–	1, 8
179	J1922 + 3920	19 22 14.7	+ 39 20 19	4.76	0.99	2.36	0.58	0.62	–	–	1, 9
180	J1926 + 4124	19 26 47.6	+ 41 24 48	7.13	0.99	0.62	0.22	0.46	–	–	1
181	J1930 – 1509	19 30 01.9	– 15 09 19	7.25	0.99	10.01	1.48	0.85	0.08	15.58	1, 15
182	J1944 + 7815	19 44 11.2	+ 78 16 18	5.56	0.99	2.80	0.56	0.72	–	–	1

Table 1 – *continued*

Cat. no.	Name	RA core (J2000.0)	Dec. core (J2000.0)	Separation (arcsec)	ρ	F_{150} (Jy)	F_{1400} (Jy)	$\alpha_{0.15}^{1.4}$ ($\pm$0.05)	z	L_{150} WHz^{-1} $\times 10^{25}$	Other catalogue
(1)	(2)	(3)	(4)	(5)	(6)	(7)	(8)	(9)	(10)	(11)	(12)
183	J1946 + 0201	19 46 4.40	+ 02 01 54	4.26	0.99	3.06	0.30	1.03	–	–	1
184	J1950 – 2817	19 50 45.9	– 28 17 39	3.37	0.99	4.25	0.62	0.86	–	–	1
185	J2000 – 0101	20 00 52.7	– 01 01 09	4.29	0.99	0.50	0.12	0.63	–	–	1, 6
186	J2015 + 1144	20 15 20.9	+ 11 44 49	2.97	0.99	0.49	0.13	0.59	–	–	1
187	J2042 – 0310	20 42 56.5	– 03 10 22	6.48	0.99	0.49	0.16	0.50	0.14	2.32	1
188	J2049 + 3526	20 49 53.2	+ 35 26 52	8.08	0.99	0.44	0.11	0.62	–	–	1, 9
189	J2102 – 0921	21 02 15.7	– 09 21 15	5.52	0.99	1.38	0.42	0.53	0.08	2.12	1
190	J2108 + 6049	21 08 41.1	+ 60 49 03	4.21	0.99	0.63	0.17	0.58	–	–	1, 8
191	J2111 + 3335	21 11 37.7	+ 33 35 12	8.49	0.99	0.63	0.11	0.78	–	–	1, 2
192	J2138 + 8307	21 38 49.8	+ 83 07 04	2.84	0.99	0.78	0.31	0.41	0.14	3.82	1, 2
193	J2139 – 3218	21 39 30.5	– 32 18 38	5.00	0.83	0.94	0.24	0.61	–	–	1, 6
194	J2144 + 8015	21 44 0.71	+ 80 15 12	4.63	0.99	0.35	0.12	0.47	–	–	1, 4
195	J2144 – 3105	21 44 04.8	– 31 05 18	1.71	0.98	0.49	0.11	0.66	0.18	4.27	1, 4
196	J2157 + 0037	21 57 31.4	+ 00 37 57	5.24	0.99	1.12	0.24	0.69	0.39[b]	54.80	1, 6
197	J2158 + 6014	21 58 46.9	+ 60 14 41	5.03	0.99	0.51	0.09	0.77	–	–	1, 8
198	J2212 + 1304	22 12 54.4	+ 13 04 36	1.60	0.99	1.76	0.07	1.44	0.15	11.54	1
199	J2300 + 1426	23 00 47.4	+ 14 26 03	4.48	0.99	1.29	0.23	0.77	0.15[b]	8.46	1
200	J2301 – 4333	23 01 17.7	– 43 33 24	4.89	0.99	1.02	–	–	–	–	6, 14
201	J2310 + 0734	23 10 22.6	+ 07 34 53	9.33	0.99	0.62	0.04	1.22	0.04	0.03	1
202	J2322 + 4157	23 22 43.3	+ 41 58 14	7.32	0.99	1.09	0.39	0.46	0.11[a]	3.82	1
203	J2348 + 0043	23 48 23.9	+ 00 43 47	1.17	0.99	0.66	0.09	0.89	0.36	28.63	1, 2, 11

Notes. 1, NVSS (Condon et al. 1990); 2, VLSS (Cohen et al. 2007); 3, 4C (Pilkington & Scott 1965; Gower, Scott & Wills 1967; Caswell & Crowther 1969); 4, 6C (Baan & McKee 1985; Hales, Baldwin & Warner 1988; Hales et al. 1990, 1991; Hales, Baldwin & Warner 1993a; Hales et al. 1993b); 5, 7C (McGilchrist et al. 1990; Kollgaard et al. 1994; Waldram et al. 1996; Vessey & Green 1998); 6, PMN (Griffith et al. 1994); 7, PKS (Bolton, Gardner & Mackey 1964); 8, 87GB (Gregory & Condon 1991); 9, B2 (Colla et al. 1970, 1972, 1973; Fanaroff & Riley 1974); 10, B3 (Ficarra, Grueff & Tomassetti 1985); 11, VFK (Van Velzen, Falcke & Körding 2015); 12, CRATES (Healey et al. 2007); 13, FIRST (Becker, White & Helfand 1995); 14, SUMSS (Mauch et al. 2003); 15, 2MASS (Skrutskie et al. 2006); 16, MG2 (Bennett et al. 1986); 17, MRC (Large et al. 1981); 18, SSTSL (Randall et al. 2012).

[a] Represents photometric redshift.

[b] Represent spectroscopic redshift.

α is the spectral index and F_ν is the radiative flux density at a given frequency ν. These spectral indices have been determined by integrating fluxes over the same aperture at both frequencies, using the formula

$$\alpha = \frac{\log F_{\nu_1} - \log F_{\nu_2}}{\log \nu_2 - \log \nu_1}. \quad (1)$$

The integrated radio flux density of tailed radio sources can be estimated using Astronomical Imaging Processing Software (AIPS) with TVSTAT. To measure the flux density in the TGSS and NVSS fields, for uniformity, we use a region corresponding to the 10.5-mJy beam^{-1} (3σ) contour level from TGSS.

The spectral index (α_{150}^{1400}) is provided in Tables 1 and 2. Spectral index measurements are available for 188 WATs and for 51 NATs. The remaining 15 WATs and 10 NATs were not detectable in NVSS maps because their declination is less than the NVSS coverage. Out of the 188 WATs with spectral index information, 13 (7 per cent) show a flat spectrum ($\alpha_{150}^{1400} < 0.5$). Out of the 51 NATs with spectral index information, 5 ($\sim$10 per cent) show a flat spectrum ($\alpha_{150}^{1400} < 0.5$). Most of the WATs and NATs show a steep radio spectrum ($\alpha_{150}^{1400} > 0.5$), which is a common property of lobe-dominated radio galaxies. The uncertainty of spectral index measurements arising from flux density uncertainty (Mahony et al. 2016) is

$$\Delta\alpha = \frac{1}{\ln \frac{\nu_1}{\nu_2}} \sqrt{\left(\frac{\Delta S_1}{S_1}\right)^2 + \left(\frac{\Delta S_2}{S_2}\right)^2}, \quad (2)$$

where $F_{\nu_{1,2}}$ and $S_{1,2}$ refer to NVSS and TGSS frequencies and flux densities respectively. The flux density accuracy in TGSS ADR 1 and NVSS is $\sim$10 per cent (Intema et al. 2017) and $\sim$5 per cent (Condon et al. 1990), respectively. Using equation (2), the spectral index uncertainty is $\Delta\alpha = 0.05$. The spectral index distributions for WATs (left-hand panel) and NATs (right-hand panel) for sources presented in this paper are shown in Fig. 4. The distributions show slightly different peaks for WATs and NATs. The distribution peaks near 0.6−0.7 for WATs and near 0.65−0.75 for NATs. For WATs, the total span of α_{150}^{1400} is from 0.02 to 1.86, and for NATs, the total span of α_{150}^{1400} is from 0.38 to 2.04. Among WATs, J0752 + 0814 has the highest spectral index (with $\alpha_{150}^{1400} = 1.70$), and J0041 + 2104 has the lowest spectral index (with $\alpha_{150}^{1400} = 0.02$). For NATs, J0704 + 6318 has the highest spectral index (with $\alpha_{150}^{1400} = 2.04$), and J2144 + 2107 has the lowest spectral index (with $\alpha_{150}^{1400} = 0.38$). The radio spectral index is commonly utilized to differentiate between source components such as the core and lobe. To ensure the location of the core, we computed the spectral index of the probable core region (found from the optical/IR counterpart and radio morphology) using the TGSS and FIRST survey (when available) and found that all of them show a flat spectral index ($\alpha_{150}^{1400} < 0.5$). The spectral index of the core is shown in images of all sources, when corresponding FIRST images are available.

4.2 Luminosity feature

We calculated the radio luminosities (L_{150}) of sources using the redshift information of either the optical counterpart or the associated galaxy cluster using the standard formula (Donoso, Best &

Table 2. Candidate NAT radio sources.

Cat. no.	Name	RA core (J2000.0)	Dec. core (J2000.0)	Separation (arcsec)	ρ	F_{150} (Jy)	F_{1400} (Jy)	$\alpha_{0.15}^{1.4}$ ($\pm$0.05)	z	L_{150} WHz^{-1} $\times 10^{25}$	Other catalogue
(1)	(2)	(3)	(4)	(5)	(6)	(7)	(8)	(9)	(10)	(11)	(12)
1	J0003 + 5745	00 03 18.9	+ 57 45 28	7.33	0.99	0.43	0.16	0.44	–	–	8
2	J0041 – 0922	00 41 30.9	– 09 22 33	7.23	0.99	10.5	–	–	–	–	17
3	J0041 – 4346	00 41 29.5	– 43 47 05	4.27	0.99	0.73	–	–	–	–	18
4	J0102 – 0050	01 02 39.8	– 00 50 41	2.32	0.99	0.43	0.13	0.53	–	–	1, 11
5	J0141 + 1623	01 41 35.5	+ 16 23 36	4.87	0.99	1.05	0.16	0.84	–	–	1, 8
6	J0148 – 3155	01 48 15.4	– 31 55 20	3.23	0.99	0.73	0.08	0.97	0.14	9.42	1
7	J0223 + 4300	02 23 19.4	+ 42 59 47	4.72	0.99	20.1	5.56	0.57	0.02	17.88	10
8	J0228 – 2814	02 28 26.0	– 28 14 13	4.14	0.99	3.45	0.68	0.72	0.20	17.38	1
9	J0236 + 1202	02 36 26.5	+ 12 02 51	1.14	0.93	0.49	0.06	0.94	–	–	1
10	J0303 + 6605	03 03 0.44	+ 66 05 43	4.45	0.99	2.38	0.33	0.88	–	–	1
11	J0303 + 1610	03 03 57.7	+ 16 10 41	5.77	0.99	0.74	0.29	0.41	–	–	1
12	J0335 + 6517	03 35 9.20	+ 65 17 04	1.10	0.81	0.38	0.20	0.28	–	–	1
13	J0411 + 6133	04 11 50.0	+ 61 33 10	1.72	0.99	1.18	0.23	0.73	–	–	1
14	J0516 + 3531	05 16 19.7	+ 35 31 49	4.09	0.99	0.46	0.12	0.60	–	–	1
15	J0523 + 2427	05 23 34.9	+ 24 27 27	10.1	0.98	0.96	0.20	0.70	–	–	9
16	J0541 + 2842	05 41 13.4	+ 28 42 47	10.7	0.91	7.24	1.40	0.73	–	–	1, 3
17	J0549 – 2520	05 49 21.6	– 25 20 47	4.61	0.99	0.75	0.20	0.59	0.04	0.27	1, 2
18	J0603 + 5108	06 03 53.9	+ 51 08 29	7.33	0.99	1.28	0.21	0.80	–	–	1
19	J0603 + 5619	06 03 28.0	+ 56 19 29	9.14	0.99	6.36	0.01	1.74	–	–	1
20	J0704 + 6318	07 04 28.7	+ 63 18 39	4.43	0.99	6.67	0.03	2.04	0.09	14.87	1, 2
21	J0709 + 5100	07 09 53.2	+ 51 00 58	1.78	0.99	1.32	0.16	0.94	–	–	1, 8, 11
22	J0728 – 0008	07 28 50.3	– 00 08 21	7.39	0.99	3.49	0.78	0.67	–	–	–
23	J0730 + 4051	07 30 43.3	+ 40 51 52	1.83	0.93	0.93	0.54	0.24	0.12[b]	3.22	1, 11
24	J0735 + 2510	07 35 42.3	+ 25 10 16	10.6	0.96	2.08	0.23	0.98	–	–	1, 11
25	J0802 + 6345	08 02 02.5	+ 63 45 55	3.27	0.99	0.78	0.07	0.98	0.07[a]	1.18	4, 11, 14
26	J0810 – 4923	08 10 42.6	– 49 23 54	5.12	0.99	11.1	–	–	–	–	–
27	J0815 + 3710	08 15 45.6	+ 37 10 24	6.34	0.96	0.51	0.13	0.61	–	–	4
28	J0818 – 0004	08 19 0.50	– 00 04 57	4.94	0.99	0.42	0.06	0.87	–	–	1
29	J0928 + 4854	09 28 22.1	+ 48 54 33	6.00	0.80	0.64	0.11	0.78	–	–	1, 4, 8
30	J0953 + 7057	09 53 59.7	+ 70 57 34	2.93	0.99	4.88	0.26	1.31	0.18[a]	47.33	1, 4, 8
31	J1108 – 4823	11 08 51.0	– 48 23 50	1.81	0.99	1.02	–	–	–	–	14
32	J1111 + 4050	11 11 39.7	+ 40 50 24	1.21	0.79	6.65	0.98	0.85	0.07[b]	7.91	11, 13
33	J1122 + 2124	11 22 30.5	+ 21 24 45	3.46	0.99	2.91	0.62	0.69	0.16	19.75	11
34	J1146 – 5236	11 46 30.1	– 52 36 39	4.91	0.99	1.23	–	–	–	–	6
35	J1202 + 8522	12 02 11.4	+ 85 22 18	3.95	0.99	0.61	0.13	0.69	–	–	1, 4
36	J1215 – 3905	12 15 18.6	– 39 05 17	10.5	0.94	1.43	0.19	0.90	–	–	1, 6
37	J1236 – 3535	12 36 45.1	– 35 35 14	0.75	0.99	0.81	0.09	0.98	0.07[b]	–	1
38	J1240 – 3413	12 40 03.7	– 34 13 29	10.7	0.99	0.89	–	–	0.07	–	1
39	J1255 – 4447	12 55 57.3	– 44 47 54	5.12	0.92	0.53	–	–	–	–	14
40	J1259 – 4458	12 59 45.6	– 44 58 37	3.21	0.99	4.29	–	–	–	–	7, 14
41	J1303 + 3150	13 03 15.5	+ 31 50 18	1.81	0.61	2.15	0.20	1.06	0.16	28.22	1,2
42	J1306 + 4633	13 06 45.7	+ 46 33 29	3.89	0.99	3.24	0.21	1.22	0.22[b]	48.89	1, 2
43	J1347 – 3905	13 47 39.3	– 39 05 42	7.23	0.99	0.42	0.04	1.05	–	–	1
44	J1409 + 7753	14 09 26.0	+ 77 53 17	2.53	0.99	0.41	0.11	0.58	–	–	1
45	J1425 + 1210	14 25 15.2	+ 12 10 09	4.47	0.99	1.38	0.49	0.46	0.15	7.89	11, 17
46	J1629 + 0104	16 29 27.3	+ 01 04 07	1.14	0.99	1.91	0.31	0.81	–	–	1
47	J1657 – 0148	16 57 52.6	– 01 48 01	5.88	0.99	1.97	0.07	1.49	–	–	1
48	J1710 + 4239	17 10 40.7	+ 42 39 45	6.94	0.99	1.54	0.46	0.54	–	–	1
49	J1924 – 0032	19 24 07.0	– 00 32 07	6.94	0.99	1.05	0.21	0.72	–	–	1, 8
50	J1926 + 4831	19 26 09.5	+ 48 31 28	3.13	0.99	1.19	0.02	1.82			1, 4
51	J1930 – 0312	19 30 57.3	– 03 12 56	8.96	0.99	0.80	0.22	0.57	–	–	1,6
52	J2038 – 2011	20 38 27.7	– 20 11 07	1.13	0.99	2.98	0.77	0.60	0.51	–	1
53	J2058 – 2125	20 58 03.8	– 21 25 19	3.55	0.97	1.14	0.11	1.04	–	–	1
54	J2104 + 1916	21 04 21.4	+ 19 16 46	4.18	0.99	3.63	0.42	0.96	–	–	1, 3
55	J2137 – 4105	21 37 51.4	– 41 05 19	7.31	0.99	2.19	–	–	0.06	–	14
56	J2144 + 2107	21 44 06.4	+ 21 07 44	2.87	0.99	0.38	0.16	0.38	–	–	1, 8
57	J2201 – 4427	22 01 58.5	– 44 27 06	2.33	0.99	1.11	–	–	–	–	6, 14
58	J2227 – 3034	22 27 54.5	– 30 34 32	2.17	0.99	3.83	0.89	0.65	0.06	0.75	1

Table 2 – *continued*

Cat. no.	Name	RA core (J2000.0)	Dec. core (J2000.0)	Separation (arcsec)	ρ	F_{150} (Jy)	F_{1400} (Jy)	$\alpha_{0.15}^{1.4}$ ($\pm$0.05)	z	L_{150} WHz^{-1} $\times 10^{25}$	Other catalogue
(1)	(2)	(3)	(4)	(5)	(6)	(7)	(8)	(9)	(10)	(11)	(12)
59	J2319 – 1838	23 19 30.0	– 18 38 05	6.12	0.99	0.45	0.15	0.49	–	–	1, 6
60	J2348 – 3117	23 48 54.9	– 31 17 32	8.80	0.99	1.14	0.33	0.55	0.18	9.75	1
61	J2351 + 0033	23 51 54.4	+ 00 33 10	4.67	0.95	0.27	0.08	0.54	0.27	5.56	1,11

Notes. 1, NVSS (Condon et al. 1990); 2, VLSS (Cohen et al. 2007); 3, 4C (Pilkington & Scott 1965; Gower et al. 1967; Caswell & Crowther 1969); 4, 6C (Baan & McKee 1985; Hales et al. 1988, 1990, 1991; Hales et al. 1993a, b); 5, 7C (McGilchrist et al. 1990; Kollgaard et al. 1994; Waldram et al. 1996; Vessey & Green 1998); 6, PMN (Griffith et al. 1994); 7, PKS (Bolton et al. 1964); 8, 87GB (Gregory & Condon 1991); 9, B2 (Colla et al. 1970, 1972, 1973; Fanaroff & Riley 1974); 10, B3 (Ficarra et al. 1985); 11, VFK (van Velzen et al. 2015); 12, FIRST (Becker et al. 1995); 13, SUMSS (Mauch et al. 2003); 14, 2MASS (Skrutskie et al. 2006); 15, MG2 (Bennett et al. 1986); 16, MRC (Large et al. 1981); 17, SSTSL (Randall et al. 2012).
[a] Represents photometric redshift.
[b] Represents spectroscopic redshift.

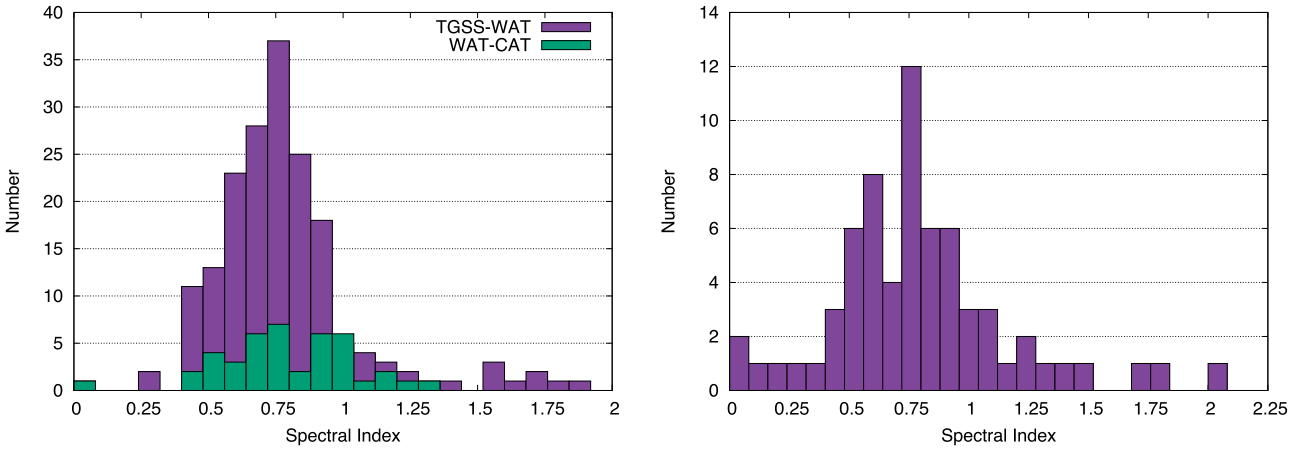

Figure 4. Histogram showing the spectral index distribution for WAT (left-hand panel) and NAT (right-hand panel) sources. We also include sources present in the WAT-CAT catalogue (Missaglia et al. 2019).

Kauffmann 2009)

$$L_{150} = 4\pi D_L^2 S_0 (1+z)^{\alpha-1}, \quad (3)$$

where z is the redshift parameter, α is the spectral index ($S \propto \nu^{-\alpha}$), D_L is luminosity distance of the source (Mpc), and S_0 is the flux density (Jy) at 150-MHz frequency.

Fig. 5 shows the redshift versus luminosity plot of the 103 tailed sources for which either the spectroscopic or the photometric redshift is available. In our sample, the highest redshifts for the NAT and WAT sources are 0.51 and 0.68, respectively. The source radio luminosities at 150 MHz are of the order of 10^{25} W Hz^{-1}, which is similar to that of a typical radio galaxy. The average value of log L [W Hz^{-1}] for WATs is 25.62 (1σ standard deviation = 0.72, median = 25.63) and that for NATs is 25.82 (1σ standard deviation = 0.72, median = 25.83). J0856 + 4829 is the least luminous WAT in our sample, with $L_{150} = 0.15 \times 10^{25}$ W Hz^{-1} ($z = 0.12$), and J0549–2520 is the least luminous NAT in our sample, with $L_{150} = 0.27 \times 10^{25}$ W Hz^{-1} ($z = 0.04$). J0225 + 4031 is the most luminous WAT in our sample, with $L_{150} = 1.9 \times 10^{27}$ W Hz^{-1} ($z \sim 0.65$), and J1314 + 6220 is the most luminous NAT in our sample, with $L_{150} = 162.8 \times 10^{25}$ W Hz^{-1} ($z = 0.14$).

4.3 Bending angle

We measured the bending angle of all sources using the angle (2θ) between two individual jet axes connecting the core, as shown in Fig. 6. We classified all tailed sources in our sample into two groups – WAT or NAT galaxy, depending on the bending angle of these sources. For some sources, the bending angle could not be measured because of the complex structure of these sources. Fig. 7 presents the distribution of bending angles of sources considered in this paper for both NAT- and WAT-type sources. Most of the NAT sources make an angle greater than 80°. WAT sources produce a wide variety of angles between the two components, with a peak near 110°–120°.

4.4 Cluster association

In the Universe, clusters are the largest gravitationally bound structures (Wen, Han & Liu 2012). Clusters provide an ideal tool for cosmologists to understand the composition and evolution of the structures of the Universe (Allen, Evrard & Mantz 2011; Wetzel, Tinker & Conroy 2012). They provide strong proof for the appearance of large amounts (80 per cent) of dark matter (Wen et al. 2012). They are created around dark matter concentrations when two cosmic objects (sheets and filaments) intersect. Understanding clusters is very helpful for tracing the large-scale structure of the Universe (Prestage & Peacock 1988; Hill & Lilly 1991; Worrall & Birkinshaw 2000; Belsole et al. 2007; Tasse et al. 2008). We associated our tailed radio galaxy sample with cluster catalogues from the literature that cover the TGSS field. These clusters have been detected using various methods, including optical, IR, X-ray, and Sunyaev-Zel'dovich (SZ) observations. The cluster catalogues used are listed in Tables 3 and

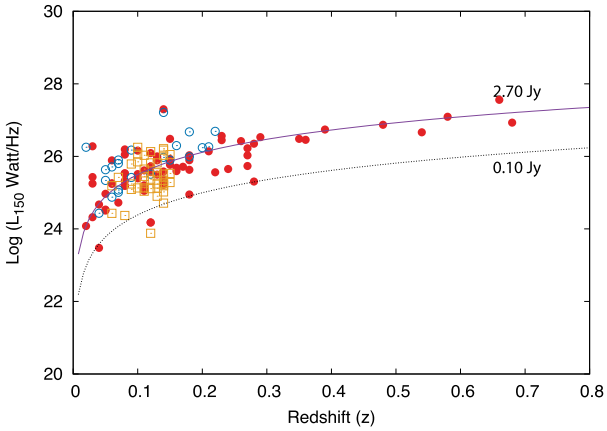

Figure 5. Plot of radio luminosity against redshift for the 103 tailed sources presented in this paper. The WAT and NAT sources are indicated by red circles and open blue circles, respectively. The yellow squares represent WAT radio galaxies in the WATCAT catalogue (Missaglia et al. 2019). The pink solid line indicates the best-fitting luminosity using points from all surveys in the figure, which corresponds to a flux density of 2.70 Jy for tailed radio sources.

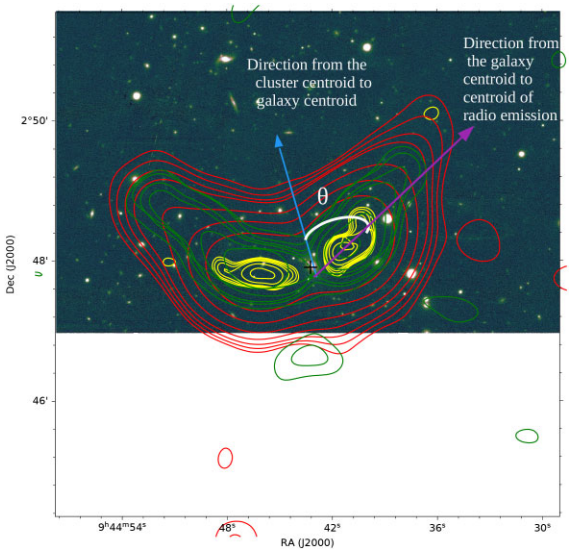

Figure 6. An example of a measurement of the bending angle of a tailed radio source. PanSTARRS *r*-band optical images are overlaid by TGSS (green contour), NVSS (red contour), and FIRST (yellow contour) images. The plus symbol is the position of the host galaxy from the PanSTARRS *r* band where the two radio tails terminate. The blue arrow indicates the direction from the cluster centroid to the galaxy centroid, and the magenta arrow shows the direction from the galaxy centroid to the centroid of the radio emission peak in the intensity map. We calculate the angle θ between the two arrows. Then, 2θ is the bending angle between the two radio tails.

4. Using only the 107 WAT and NAT sources with redshifts, we performed a three-dimensional cross-match with the known clusters across the field using a search radius of 2 Mpc. The distance was computed using the source redshift. We assumed that tailed radio galaxies and clusters of galaxies are associated if $\Delta z = |z - z_{\rm spec}| \leq 0.005$, where $z_{\rm spec}$ is the spectroscopic redshift of the galaxy cluster (Moore, Frenk & White 1993; Eke 2004; Berlind, Frieman & Weinberg 2006). We found associated known clusters or groups for 120 tailed radio galaxies from our WAT and NAT sample (out of a total of 264). The details of associated clusters for WATs and NATs

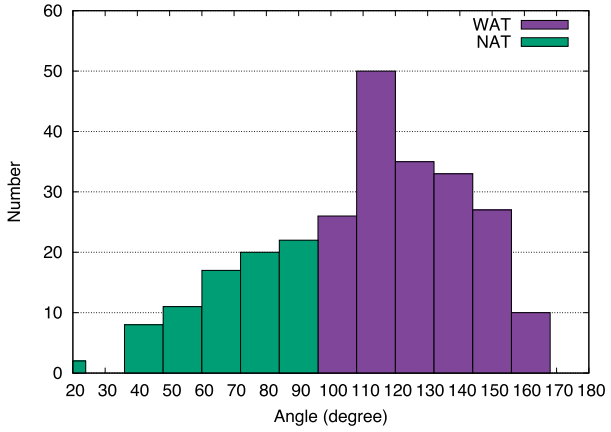

Figure 7. Distribution showing the source count versus bending angle of the tailed galaxies. The green and blue bars indicate the number of NAT and WAT sources, respectively, in the range of a particular bending angle.

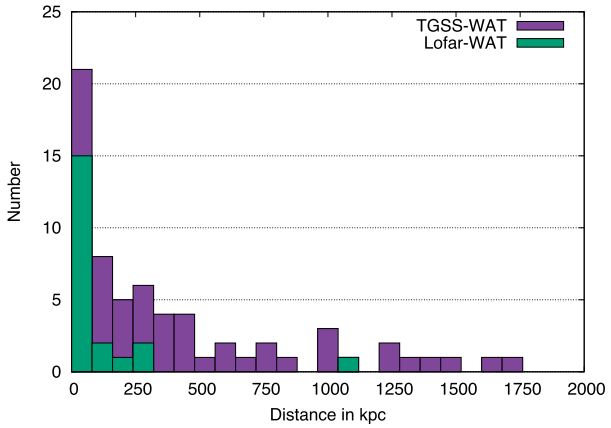

Figure 8. Distribution of the distance of tailed radio galaxies from the galaxy cluster centre. Sources presented in LoFAR WATs (Pal & Kumari 2022) are included.

considered in this paper are listed in Tables 3 and 4. In columns (1) and (2), the catalogue number and galaxy cluster identification name are given. In columns (3) and (4), the name of the catalogue in which the cluster is named and the redshift of the cluster are given. Column (5) and (6) contain the comoving distance ($D_{\rm c}$) in Mpc at the source redshift and the angular separation (in arcseconds) between the centre of the associated cluster and the galaxy centre. Column (7) indicates the linear distance of the host galaxy from the cluster centre. In column (8), the Brightest Cluster Galaxy (BCG) *r*-band magnitude m_r is shown. Column (9) and (10) give the cluster radius (r_{500}) and cluster richness (R_L). In column (11), the number of member galaxy candidates (N_{500}) within r_{500} is shown, and in column (12), the mass of the cluster within r_{500} (M_{500}) is presented. The cluster density ($\rho_{\rm co}$) is provided in column (13).

For the purposes of having a homogeneous study, various parameters (m_r, r_{200}, N_{500}, and R_L) of clusters in Tables 3 and 4 were collected from Wen et al. (2012) and Wen & Han (2015). We calculated the optical mass M_{500} and cluster density $\rho_{\rm co}$ using these parameters. We also found that for 65 tailed radio sources in our sample, the distance between the two sources is less than 500 kpc. Searches for new clusters of galaxies are recommended near those WATs and NATs when no associated cluster has been identified.

Table 3. Cluster details for candidate WAT radio sources.

Cat. no.	Name	Cluster	z_{cl}	(D_c) (Mpc)	θ (arcsec)	D (kpc)	m_r	r_{500} (Mpc)	R_L	N_{500}	M_{500} $\times 10^{14}$ $M_\odot$	ρ_{co} (Mpc^{-3})
1	J0003 – 3556	ABELL 2717	0.05	218.4	36.9	133.8	–	–	–	–	–	–
2	J0022 + 2317	RM J002224.7 + 231733.0	0.13	556.6	4.8	41.2	–	–	–	–	–	–
3	J0030 + 1058	NSCS J003033 + 105852	–	–	78.0	–	–	–	–	–	–	–
4	J0054 + 3339	ZwCl 0051.7 + 3322	–	–	222.0	–	–	–	–	–	–	–
5	J0114 + 0029	WHL J011425.6 + 002933	0.34	1377	0.6	10.7	18.36	0.82	39.20	19	2.25	53.0
6	J0120 + 1451	YSS2008 466	0.05	218.4	162.0	586.7	–	–	–	–	–	–
7	J0123 + 3315	MCXC J0123.6 + 3315	0.02	88.0	21.6	31.6	–	–	–	–	–	–
8	J0128 + 3448	WHL J012859.1 + 344842	0.15	639.0	0.1	0.96	16.32	0.88	35.48	21	2.01	58.6
9	J0149 + 1403	MSPM 01728	0.07	304.3	3.6	17.8	–	–	–	–	–	–
10	J0204 + 0415	WHL J020431.3 + 041501	0.14	597.9	38.4	350.7	16.2	0.60	14.9	9	0.87	25.1
11	J0205 – 4124	SPT-CL J0205 – 4125	–	–	258.0	–	–	–	–	–	–	–
12	J0209 + 0950	NSC J020939 + 094834	0.09	389.3	138.0	859.1	–	–	–	–	–	–
13	J0257 – 0400	WHL J025743.7 – 035951	0.18	760.8	10.8	121.3	18.9	0.80	31.8	19	2.00	53.0
14	J0306 – 1206	ABELL 0415	0.08	346.9	294.0	1643.0	–	–	–	–	–	–
15	J0315 + 0507	WHL J031530.6 + 050746	0.22	920.2	6.0	78.9	17.3	0.69	17.5	9	1.04	25.1
16	J0317 + 1212	WHL J031723.6 + 121234	0.22	920.2	6.0	78.9	16.4	1.01	53.5	16	3.55	44.7
17	J0522 + 2807	WHL J052246.0 + 280640	0.13	556.6	19.2	164.7	14.7	0.89	39.6	16	2.55	44.7
18	J0631 + 2500	PSZ2 G188.38 + 07.05	0.08	346.9	55.8	311.8	–	–	–	–	–	–
19	J0708 + 7152	WHL J070819.0 + 715224	0.11	473.4	67.8	503.9	15.3	–	57.2	–	3.49	–
20	J0733 + 4211	WHL J073312.6 + 421156	0.48	1870.5	6.0	132.2	19.0	0.85	12.5	18	0.62	6.44
21	J0736 + 2412	WHL J073618.1 + 241043	0.14	597.9	107.0	977.4	16.2	0.75	29.9	16	1.87	44.7
22	J0757 + 3640	WHL J075753.2 + 364022	0.12	515.1	3.0	24.1	15.6	0.70	17.6	16	1.04	44.7
23	J0805 + 1614	WHL J080543.1 + 161356	0.10	431.4	5.4	36.9	15.8	0.76	21.7	14	1.31	39.1
24	J0818 + 5437	WHL J081803.9 + 543709	0.10	431.4	18.0	123.0	14.9	1.01	56.8	29	3.79	81.0
25	J0856 + 4829	WHL J085600.8 + 482910	0.12	515.1	10.2	81.8	15.8	0.95	44.3	25	2.89	69.8
26	J0912 + 1600	NSC J091232 + 155800	0.19	801.0	120.0	1409.0	–	–	–	–	–	–
27	J0917 + 5509	WHL J091708.0 + 550908	0.19	801.0	0.2	2.4	16.27	0.79	33.56	15	1.89	41.9
28	J0944 + 0247	WHL J094443.2 + 024754	0.21	880.7	0.4	5.07	16.59	1.12	91.99	46	5.62	128.5
29	J1012 + 0841	WHL J101206.4 + 084133	0.09	389.3	0.2	1.3	15.78	0.65	11.72	10	0.52	27.93
30	J1015 + 1221	WHL J101540.7 + 122030	0.61	2292.6	31.2	774.8	20.4	0.70	28.7	8	1.79	22.3
31	J1019 + 7020	WHL J101956.5 + 702034	0.24	–	53.4	–	17.4	–	70.1	–	4.37	–
32	J1022 + 5006	WHL J102228.4 + 500620	0.15	639.0	0.1	0.9	15.27	1.32	119.33	74	7.46	206.7
33	J1032 + 3151	WHL J103214.4 + 315214	0.35	1413.6	54.6	996.9	17.8	1.00	55.4	26	3.69	72.6
34	J1034 + 0736	WHL J103409.1 + 073616	0.45	1768.2	13.2	280.8	–	–	–	–	–	–
35	J1042 + 0237	NSC J104200 + 023739	0.04	175.2	4.2	12.3	–	–	–	–	–	–
36	J1046 – 2911	ABELL S0646	0.06	261.5	19.8	85.0	14.31	–	17.2	–	0.93	–
37	J1048 + 3532	RM J104851.5 + 353136.4	0.36	1450.0	39.0	725.4	19.1	–	–	–	–	–
38	J1050 + 0432	MaxBCG J162.734 + 4.525	0.12	515.1	81.6	654.5	–	–	–	–	–	–
39	J1050 – 2405	MCXC J1050.6 – 2405	0.20	840.9	26.4	322.4	–	–	–	–	–	–
40	J1051 + 1825	NSC J105152 + 182302	0.11	473.4	180.0	1338.0	–	–	–	–	–	–
41	J1056+ 0255	WHL J105617.0 + 025526	0.39	1558.0	0.1	1.9	18.92	0.70	27.38	14	1.52	39.1
42	J1058 + 0136	SDSS-C4 1110	0.04	175.2	53.4	156.7	13.6	–	28.9	–	1.64	–
43	J1118 + 2754	NSC J111853 + 275216	0.06	261.5	132.0	566.9	–	–			–	–
44	J1119 + 6317	WHL J111933.1 + 631717	0.16	679.8	0.6	6.1	15.68	0.76	26.27	16	1.45	44.7
45	J1120 + 2912	WHL J112038.5 + 291234	0.27	1114.4	2.2	33.1	17.0	0.73	21.0	11	1.27	30.7
46	J1130 + 2524	WHL J113048.8 + 252436	0.15	639.0	1.8	17.4	16.2	0.71	20.5	16	1.23	44.7

Table 3 – *continued*

Cat. no.	Name	Cluster	z_{cl}	(D_c) (Mpc)	θ (arcsec)	D (kpc)	m_r	r_{500} (Mpc)	R_L	N_{500}	M_{500} $\times 10^{14}$ $M_\odot$	ρ_{co} (Mpc^{-3})
47	J1132 + 6311	NSC J113242 + 631204	0.10	431.4	60.6	414.2	–	–	–	–	–	–
48	J1142 + 1102	WHL J114254.3 + 110133	0.15	639.0	33.0	325.5	16.0	1.13	82.6	46	5.37	128.5
49	J1151 + 0422	NSC J115145 + 042203	0.13	556.6	0.4	3.4	–	–	–	–	–	–
50	J1155 + 5755	WHL J115556.3 + 575501	0.16	679.8	29.4	300.2	16.5	0.84	28.0	18	1.74	50.2
51	J1156 + 3432	GMBCG J179.0225 + 34.55	0.26	1076.0	29.4	437.9	1.52	–	–	–	–	–
52	J1202 + 5802	WHL J120203.8 + 580207	0.09	389.3	1.0	6.2	15.2	0.94	46.1	30	3.02	83.8
53	J1205 + 3204	WHL J120514.5 + 320417	0.17	720.4	0.2	2.2	16.52	0.87	–	–	–	–
54	J1206 + 3152	WHL J120647.7 + 315231	0.15	639.0	0.6	5.8	16.90	0.77	29.65	14	1.65	39.1
55	J1242 + 5021	WHL J124207.4 + 502147	0.15	639.0	0.4	3.8	16.33	0.52	10.28	5	0.53	13.96
56	J1249 + 0144	WHL J124943.7 + 014447	0.20	840.9	31.4	383.4	16.9	0.98	52.8	38	1.50	106.1
57	J1304 + 6439	WHL J130428.8 + 643937	0.23	959.4	1.0	13.6	16.3	0.79	29.3	13	1.83	36.3
58	J1307 + 5651	MaxBCGJ196.932 + 56.850	0.23	959.4	0.3	4.1	–	–	–	–	–	–
59	J1311–0120	WHL J131132.1 – 011946	0.17	720.4	15.0	161.0	–	–	–	–	–	–
60	J1315 + 4841	WHL J131527.6 + 484025	0.48	1870.5	56.8	1252.0	19.8	1.03	81.9	39	5.68	108.9
61	J1321 + 4235	MSPM 05039	0.08	346.9	83.5	468.0	–	–	–	–	–	–
62	J1325 + 5736	WHL J132511.2 + 573601	0.12	515.1	6.6	52.9	14.1	1.03	109.4	59	7.81	164.8
63	J1331 – 0544	ABELL 1751	0.15	642.8	90.0	243.7	16.2	–	34.2	–	1.98	–
64	J1412 + 7420	ABELL 1893	0.21	880.7	133.2	1689.0	–	–	–	–	–	–
65	J1414 + 0143	MSPM 01989	0.05	218.4	79.0	286.1	–	–	–	–	–	–
66	J1416 + 0219	NSC J141606 + 021843	0.15	639.0	108.1	1046.8	–	–	–	–	–	–
67	J1440 + 0328	WBL 518	0.02	88.0	12.1	18.0	–	–	–	–	–	–
68	J1449 + 3959	WHL J144900.9 + 400044	0.19	801.0	84.0	986.3	16.8	0.66	18.5	13	1.10	36.3
69	J1450 + 4418	WHL J145039.8 + 441829	0.27	1114.4	3.6	55.1	17.5	1.02	73.1	36	5.01	100.5
70	J1509 + 3327	WHL J150959.8 + 332746	0.11	473.4	1.2	10.1	–	–	–	–	–	–
71	J1553 + 1530	ZwCl 1551.4 + 1539	0.14	597.9	1.0	10.2	–	–	–	–	–	–
72	J1604 + 2355	WHL J160456.7 + 235558	0.05	218.4	1.3	5.6	12.7	–	15.0	–	0.80	–
73	J1612 + 2929	MSPM 00091	0.03	131.7	83.0	184.1	–	–	–	–	–	–
74	J1615 + 4711	WHL J161541.3 + 471004	0.20	840.9	104.6	1278.8	17.0	0.83	33.3	20	2.11	55.8
75	J1616 + 0926	WHL J161653.2 + 092635	0.20	840.9	0.8	9.8	–	–	–	–	–	–
76	J1636 + 2718	WHL J163604.2 + 271829	0.13	556.6	14.4	123.5	15.7	0.74	22.4	14	1.36	39.1
77	J1711 + 1351	WHL J171150.9 + 135151	0.23	959.4	1.0	13.6	16.1	0.83	33.6	12	2.13	33.5
78	J1717 + 3734	WHL J171725.4 + 373458	0.09	389.3	0.6	3.7	–	–	–	–	–	–
79	J1735 + 3137	RM J173507.0 + 313755.5	0.26	1076.0	7.5	130.3	17.8	–	26.8	–	2.33	–
80	J1930 – 1509	MCXC J1930.0 – 1509	0.08	346.9	26.3	147.4	14.4	–	32.7	–	1.88	–
81	J2138 + 8307	ABELL 2387	0.14	597.9	29.3	268.1	–	–	–	–	–	–
82	J2139 – 3218	APMCC 693	0.08	348.9	105.8	165.6	17.0	–	39.6	–	2.33	–
83	J2144 – 3105	EDCC 027	0.18	765.4	114.4	196.7	16.9	–	31.1	–	1.78	–
84	J2212 + 1304	MaxBCG J333.226 + 13.076	0.15	639.0	0.1	0.96	–	–	–	–	–	–
85	J2226 + 1721	ABELL 2443	0.11	473.4	62.6	465.3	14.9	–	52.5	–	3.18	–
86	J2300 + 1426	WHL J230046.8 + 142602	0.15	639.0	1.2	10.6	–	–	–	–	–	–
87	J2310 + 0734	Pegasus II CLUSTER	0.04	75.2	58.0	12.0	13.3	–	45.8	–	2.73	–
88	J2322 + 4157	ZwCl 2322.4 + 4157.6	–	–	486.0	–	–	–	–	–	–	–
89	J2348 + 0043	SDSS CE J357.08 + 00.73	0.39	1558.0	61.0	1192.7	–	–	–	–	–	–

Table 4. Cluster details for candidate NAT radio sources.

Cat. no.	Name	Cluster	z_{cl}	(D_c) (Mpc)	θ (arcsec)	D (kpc)	m_r	r_{500} (Mpc)	R_L	N_{500}	M_{500} $\times 10^{14}$ $M_\odot$	ρ_{co} (Mpc^{-3})
1	J0013 – 1930	WHY J001334.0 – 192902	0.09	389.3	132.6	826.1	15.1	–	92.5	–	6.49	–
2	J0041 – 0922	ABELL 0085	0.05	218.4	108.6	394.0	–	–	–	–	–	–
3	J0041 – 4346	ABELL 2809	0.15	639.0	190.8	1849.4	15.9	–	23.0	–	1.28	–
4	J0102 – 0050	NSCS J010240 – 005003	0.25	1037.3	41.4	599.1	17.5	–	34.6	–	–	–
5	J0148 – 3155	ABELL 2943	0.14	597.9	16.8	153.4	16.3	–	88.3	–	5.63	–
6	J0228 – 2814	ABELL 3023	0.21	880.7	67.2	852.5	–	–	–	–	–	–
7	J0653 + 6919	RX J0653.4 + 6919	0.15	639.0	69.0	668.8	–	–	–	–	–	–
8	J0704 + 6318	ABELL 0556	0.09	389.3	34.2	212.9	15.1	–	82.2	–	5.20	–
9	J0730 + 4051	WHL J073045.4 + 405038	0.12	515.1	60.0	481.2	–	–	–	–	–	–
10	J0735 + 2510	WHL J073539.8 + 251020	0.08	346.9	48.0	269.0	14.9	0.88	37.2	18	2.38	50.2
11	J0802 + 6345	NSC J080155 + 634523	0.09	389.3	53.4	332.4	–	–	–	–	–	–
12	J0953 + 7057	ABELL 0875	0.18	760.8	136.6	1534.7	16.2	–	38.5	–	2.26	–
13	J1038 – 2453	PSZ2 G268.30 + 28.89	0.12	515.1	54.2	434.7	15.4	–	–	–		–
14	J1111 + 4050	ABELL 1190	0.07	304.3	67.8	336.0	–	–	–	–	–	–
15	J1122 + 2124	WHL J112229.9 + 212422	0.15	639.0	22.8	221.0	16.4	1.16	83.7	45	5.82	125.7
16	J1236 – 3535	ABELLs 0701	0.07	304.3	196.2	972.4	14.4	–	33.2	–	1.92	–
17	J1240 – 3413	ABELL 3524	0.07	304.3	20.4	101.1	14.0	–	32.7	–	1.89	–
18	J1306 + 4633	WHL J130650.0 + 463333	0.24	998.5	44.4	623.3	16.1	1.41	165.7	87	12.33	243.0
19	J1314 + 6220	NSC J131425 + 621907	0.13	556.6	36.6	314.1	–	–	–	–	–	–
20	J1409 + 7753	NSC J140833 + 775227	0.19	801.0	108.6	1275.1	–	–	–	–	–	–
21	J1425 + 1210	NSC J142513 + 120946	0.15	639.0	38.4	372.2	–	–	–	–	–	–
22	J1446 – 0846	ABELL 1964	0.07	304.3	168.0	832.6	–	–	–	–	–	–
23	J1657 – 0148	RXSC J1657 – 0148	0.03	131.7	40.8	90.5	–	–	–	–	–	–
24	J1710 + 4239	WHL J171040.7 + 423945	0.17	720.4	14.4	154.5	16.2	0.73	26.0	17	1.60	47.5
25	J1926 + 4831	CIZA J1926.1 + 4833	0.09	389.3	67.2	418.3	15.3	–	58.0	–	3.54	–
26	J2022 – 2056	ABELL 0868	0.05	218.4	34.8	126.0	–	–	–	–	–	–
27	J2137 – 4105	APMCC 688	0.06	261.5	252.0	1082.4	–	–	–	–	–	–
28	J2227 – 3034	2PIGG J2227.0 – 3041	0.07	304.3	2.4	11.8	–	–	–	–	–	–
29	J2348 – 3117	ABELL 4043	0.18	760.8	44.0	494.3	16.4	–	66.5	–	4.12	–

5 DISCUSSION

5.1 Radio properties of WATs and NATs

Based on our study, in this section we further discuss our results for tailed radio sources. We also include other samples (WAT-CAT catalogue, LoFAR catalogue) and make a comparison with their results.

Fig. 8 shows the distribution of distance of WATs with respect to the centre of host cluster. The cluster-centric distance distribution peak is seen at a distance of <250 kpc. For distances greater than ∼600 kpc, the fraction of WATs decreases quickly. This figure shows that the majority of the WATs lie close to the cluster centre, and the number of WATs decreases with the distance from the centre of a galaxy cluster. WATs usually settle in the cluster centre, namely at the bottom of the potential well (Gunn et al. 2006). The relative velocities of WATs with respect to the background are thought to be low (Leahy & Williams 1984). It is also known that a merger between two clusters could induce shocks that pass through the radio galaxies and could also affect the wide jet morphology (Gan et al. 2017). NATs are usually field galaxies moving through their host cluster with high velocity ∼2500 km s^{-1} (e.g. NGC 1265; Sun et al. 2005). NATs and WATs originate from the same physical processes, but the jet physics are different as a result of the different environments.

Fig. 9 shows the variation of radio luminosity with the spectral index of tailed radio galaxies. The figure indicates that the spectral index tends to increase with radio power. The correlation is significant for our sample, which was selected at a low frequency of 150 MHz. This result is consistent with previous studies (Blundell, Rawlings & Willott 1999). There is a tendency for the majority of powerful radio sources to have a higher spectral index. At low frequencies, the spectral index gives us information on the energy index of the synchrotron particles that are injected into the lobes (Blundell et al. 1999). With the help of an enhanced magnetic field, radio sources create a high jet kinetic power (Blundell et al. 1999), which helps the fast synchrotron cooling of relativistic electrons. The cooling time (τ) varies with the magnetic field ($\tau \propto 1/B^2$). Finally, the magnetic field enhances the synchrotron loss and make a steeper energy distribution at high radio luminosities.

Fig. 5 represents the distribution of tailed radio sources in the log L–z plane. Most of the sources are within the redshift range of 0.1 to 0.4, and the number of radio sources decreases with increasing redshift beyond $z = 0.5$. There are no available sources in the lower right quadrant of Fig. 5, owing to the non-identification of low-luminosity radio galaxies at high redshifts. This sensitivity limit of the survey is known as the Malmquist bias (Malmquist 1922, 1936). The Malmquist bias means that there will be a tight correlation between luminosity and redshift in a single flux-limited sample. A tight correlation depends on (i) the steepness of the distribution in the jet kinetic power, and (ii) the energy distribution of the particles injected into lobes (Blundell et al. 1999). This is expected because the radio luminosity is strongly correlated with the above two parameters. At high redshifts, however, a negative correlation is established between the projected linear size and redshift.

Based on the availability of redshift data, we estimated L_{150} for 79 WATs and 21 NATs from our catalogue. The means and medians L_{150} of WATs and NATs confirm that WATs and NATs have the same distribution of the radio luminosity, which implies that the governing conditions in the core engines of WATs and NATs may be the same. The mean and median of log L_{150} [W Hz^{-1}] of WATs in Missaglia et al. (2019) are 25.40 and 25.35, and in Pal & Kumari (2022) they are 25.59 and 25.60, respectively, which indicates that our tailed radio galaxies have a similar luminosity to tailed radio galaxies in the FIRST and LOFAR catalogues.

The spectral index features of the tailed radio source population can be used to identify a variety of source characteristics. For example, the radio spectral index is commonly utilized to differentiate between the source components of active galactic nuclei. The nature of core radio spectral indices is normally flat or inverted. Inverted radiation spectra probably originate in partially optically thick regimes, where low-frequency radiation is preferentially absorbed via free–free absorption or synchrotron self-absorption. On the other hand, flat spectra probably arise from the superposition of naturally distinct regions along the jet with dynamically lower frequency turnover . Steep energy spectra usually come from lobe components, and ultra-steep energy spectra arise in the relic emission (Mahony et al. 2016). All previous studies (Mahony et al. 2016; Ishwara-Chandra, Sirothia & Wadadekar 2010; Kapahi, Athreya & van Breugel 1998) found the mean spectral index of radio galaxies in the range of 0.7–0.8 and 0.75 is usually considered to be the typical spectral index for radio galaxies. For example, Mahony et al. (2016) found radio galaxies with the spectral index in the range –0.5 to 1.5 with median = 0.78, and Ishwara-Chandra et al. (2010) found radio galaxies with the spectral index in the range –0.5 to 2.5 with median = 0.78. The mean and median of the spectral index of tailed radio sources presented in this paper is close to the spectral index of a typical radio galaxy, which implies that tailed radio galaxies and normal radio galaxies are similar in terms of the properties of their spectral index.

5.2 Cluster mass and tailed radio galaxies

The bending of jets is affected by the mass of the parent cluster in two ways. First, the cluster mass is correlated with the density of the ICM, with heavier clusters experiencing a denser ICM. Secondly, the mass of the cluster is correlated with the velocity dispersion of galaxies, which results in the faster movement of galaxies in high-mass clusters (Mguda et al. 2015). According to a simulation by Mguda et al. (2015), there are no tailed radio galaxies in clusters with masses lower than 10^{13} $M_\odot$, and only a few in clusters with masses lower than $10^{13.5}$ $M_\odot$. Another simulation suggests the presence of over 50000 galaxy clusters in the mass range 10^{13} $M_\odot$–10^{14} $M_\odot$ and over 4000 galaxy clusters with masses higher than 10^{14} $M_\odot$, which gives favourable conditions for radio jet bending (Gottlöber et al. 2006). The majority of tailed radio galaxies are seen in clusters with a mass range between 10^{14} $M_\odot$ and 10^{15} $M_\odot$. Clusters with a mass above $10^{14.5}$ $M_\odot$ are expected to host at least one tailed galaxy at some point during their lifetime (Mguda et al. 2015). In Tables 3 and 4, we summarize the different properties of clusters corresponding to the WAT and NAT galaxies detected in this paper. The mass and radius are two important properties of a cluster. The widely used parameters of a cluster are r_{500}, the radius within which the mean density of a cluster is 500 times that of the critical density of the Universe ($\rho_c = 3H^2(z)/8\pi G$), and M_{500}, the cluster mass within r_{500}. We calculated the cluster optical mass M_{500} (in unit of 10^{14} $M_\odot$) from the cluster richness (R_L), which is strongly correlated as (Wen & Han 2015)

$$\log M_{500} = (1.08 \pm 0.02) \log R_L - (1.37 \pm 0.02). \quad (4)$$

We found host clusters for 118 tailed sources using 22 known cluster catalogues, as sumnmarized in Table 5. Most of the clusters can also be found from the WHL cluster catalogue, which provides the optical richness and optical mass (M_{500}). The range of the optical mass (M_{500}) of the clusters is 0.27×10^{14} $M_\odot$ to 13.06×10^{14} $M_\odot$. Four of these clusters come from X-ray cluster catalogues. We

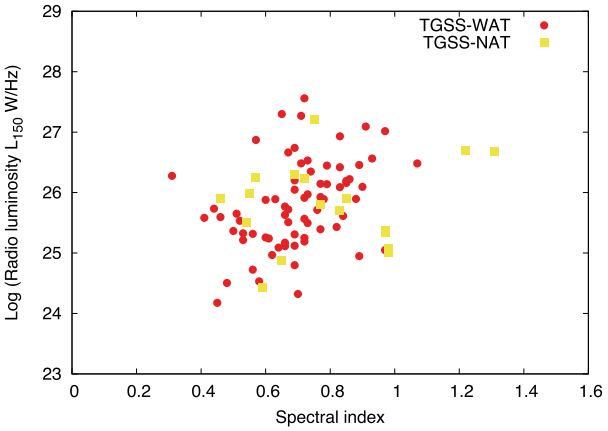

Figure 9. Variation of the spectral index with the radio luminosity of tailed radio galaxies.

calculated the corresponding optical masses of galaxy clusters from the MCXC cluster catalogue, using their optical properties from Wen et al. (2012) and Wen & Han (2015). We found that the majority (166 of a total of 284) of tailed radio galaxies in our sample have no association with known clusters or groups. The detected WAT and NAT sources should be used to search for nearby clusters. There are 10 clusters which have relatively low-mass (of the order of 10^{14} $M_{\odot}$).

6 SUMMARY

We have presented 264 new tailed radio galaxies from a visual inspection of the 150-MHz TGSS survey, out of which 203 are WAT-type and 61 are NAT-type sources. We found 192 sources from the northern sky and 72 sources from the southern sky. Because of the low radio frequency used in the survey, a significant number of steep-spectrum sources are seen.

A summary of the paper is as follows.

(i) We report a sample of 264 tailed radio galaxies. This makes it the largest sample of tailed radio galaxies discovered to date. Out of 264 new tailed galaxies, 203 are WAT-type galaxies and 61 are NAT-type galaxies.

(ii) The optical/IR counterparts of 261 sources are found, and 112 sources have an associated redshift. About 45 per cent (92/203) of WATs and 32 per cent (20/61) of NATs are identified by redshift.

(iii) The total integrated flux density of sources in our sample at 150 MHz ranges from 0.1 Jy to as high as 20.1 Jy.

(iv) In our sample of tailed radio galaxies, two tailed galaxies (WAT-J0932 + 5533 and NAT-J2038–2011) are hosted by quasars.

(v) The high-resolution deep radio observations of TGSS-ADR images have enabled us to find tailed radio galaxies with lower luminosity at 150 MHz. J0856 + 4829 is the least luminous WAT in our sample, with $L_{150} = 1.5 \times 10^{24}$ W Hz^{-1} ($z = 0.12$), and J0549–2520 is the least luminous NAT in our sample, with $L_{150} = 2.7 \times 10^{24}$ W Hz^{-1} ($z = 0.04$). J0225 + 4031 is the most luminous WAT in our sample, with $L_{150} = 1.9 \times 10^{27}$ W Hz^{-1} ($z \sim 0.65$), and J1314 + 6220 is the most luminous NAT in our sample, with $L_{150} = 162.8 \times 10^{25}$ W Hz^{-1} ($z = 0.14$).

(vi) The spectral index peaks near 0.75 for both WATs and NATs. For WATs, the total span of α_{150}^{1400} is from 0.02 to 1.70, and for NATs, the total span of α_{150}^{1400} is from 0.38 to 2.04.

(vii) The measured span of the optical mass of host galaxy clusters for M_{500} is 0.52×10^{14}–12.33×10^{14} solar mass.

(viii) The range of the calculated density of galaxy clusters is from 206.7 (Mpc^{-3}) to 36.3 (Mpc^{-3}).

Table 5. Details of various cluster surveys used in this work. The short name is used to refer to the catalogues mentioned in this paper. N is the number of clusters within the TGSS field without a redshift; N_z is the number of clusters with a redshift; and N_t is the total number of clusters.

Serial number	Catalogue name	Observation band	N_z	N	N_t	Ref.
1	ABELL	Optical	7	–	7	Abell, Corwin & Olowin (1989)
2	RM	Optical, IR	3	–	3	Rozo et al. (2015)
3	NSCS	Optical	2	–	2	Lopes et al. (2004)
4	WHL	Optical, X-ray	53	–	53	Wen & Han (2015)
5	ZwCl	Optical	1	2	3	Zwicky et al. (1961)
6	MCXC	X-ray	3	–	3	Piffaretti et al. (2011)
7	MSPM	Optical	4	–	4	Smith et al. (2012)
8	SPT-CL	SZ	–	1	1	Bleem et al. (2015)
9	CIZA	X-ray	1	–	1	Ebeling, Mullis Christopher & Tully (2002)
10	NSC	Optical	8	1	9	Gal et al. (2009)
11	SDSS-C4	Optical	1	–	1	Miller et al. (2005)
12	MaxBCG	Optical	3	–	3	Koester et al. (2007)
13	GMBCG	Optical	1	–	1	Hao et al. (2010)
14	APMCC	Optical	2	–	1	Dalton et al. (1997)
15	EDCC	Optical	1	–	1	Lumsden et al. (1992)
16	Pegasus	Optical	1	–	1	Chincarini & Rood (1976)
17	RX	X-ray	1	–	1	McGlynn et al. (2004)
18	2PIGG	IR	1	–	1	Eke et al. (2004)
19	YSS	Optical	1	–	1	Yoon et al. (2008)
20	PSZ2	Radio	2	–	2	Khatri et al. (2016)
21	RXSC	X-ray	1	–	1	Chon, Bohringer & Nowak (2013)
22	WBL	Optical	1	–	1	White et al. (1999)

ACKNOWLEDGEMENTS

We thank the whole TGSS team and the staff of the GMRT behind this survey. GMRT is run by the National Centre for Radio Astrophysics of the Tata Institute of Fundamental Research. This research has made use of the 'Aladin Sky Atlas' developed at CDS, Strasbourg Observatory, France and the NASA/IPAC Extragalactic Database (NED) operated by the Jet Propulsion Laboratory, California Institute of Technology. This publication makes use of data products from the Two Micron All Sky Survey, which is a joint project of the University of Massachusetts and the Infrared Processing and Analysis Center/California Institute of Technology, funded by the National Aeronautics and Space Administration and the National Science Foundation.

DATA AVAILABILITY STATEMENT

The data that support the plots within this paper and other findings of this study are available from the corresponding author upon reasonable request. The TGSS ADR 1 images are available at http://tgssadr.strw.leidenuniv.nl/doku.php.

REFERENCES

Abell G. O., Corwin H. G. Jr, Olowin R. P., 1989, ApJS, 70, 1
Adams M., Jensen E., Stocke J., 1980, AJ, 85, 1010
Aghanim N. et al., 2020, A&A, 641, A6
Alam S. et al., 2015, ApJS, 219, 12
Allen S. W., Evrard A. E., Mantz A. B., 2011, ARA&A, 49, 409
Baan W. A., McKee M. R., 1985, A&A, 143, 136
Becker R. H., White R. L., Helfand D. J., 1995, ApJ, 450, 559
Begelman M. C., Rees M. J., Blandford R. D., 1979, Nature, 279, 770
Belsole E., Worrall D. M., Hardcastle M. J., Croston J. H., 2007, MNRAS, 381, 1109
Bennett C. L., Lawrence C. R., Burke B. F., Hewitt J. N., Mahoney J., 1986, ApJS, 61, 1
Berlind A. A. et al., 2006, ApJS, 167, 1
Bhukta N., Mondal S. K., Pal S., 2022a, preprint (arXiv:astro-ph:2201.12353)
Bhukta N., Pal S., Mondal S., 2022b, MNRAS, 512, 4308
Blanton E. L., Gregg M. D., Helfand D. J., Becker R. H., White R. L., 2000, ApJ, 531, 118
Blanton E. L., Gregg M. D., Helfand D. J., Becker R. H., Leighly K. M., 2001, AJ, 121, 2915
Blanton E. L., Gregg M. D., Helfand D. J., Becker R. H., White R. L., 2003, AJ, 125, 1635
Bleem L. E. et al., 2015, ApJS, 216, 27
Bliton M., Rizza E., Burns J. O., Owen F. N., Ledlow M. J., 1998, MNRAS, 301, 609
Blundell K. M., Rawlings S., Willott C. J., 1999, AJ, 117, 677
Bolton J., Gardner F., Mackey M., 1964, Australian J. Phys., 17, 340B
Bridle A. H., Fomalont E. B., Palimaka J. J., Willis A. G., 1981, ApJ, 248, 499
Burns J. O., 1981, MNRAS, 195, 523
Burns J. O., Balonek T. J., 1982, ApJ, 263, 546
Burns J. O., Eilek J. A., Owen F. N., 1982, in Heeschen D., Wade C., eds, IAU Symp. 97, Extragalactic Radio Sources. Reidel, Dordrecht, p. 45
Burns J. O., O'Dea C. P., Gregory S. A., Balonek T. J., 1986, ApJ, 307, 73
Caswell J. L., Crowther J. H., 1969, MNRAS, 145, 181
Chambers K. C., Magnier E. A., Metcalfe N. et al., 2016, preprint (arXiv:1612.05560)
Chincarini G., Rood H. J., 1976, PASA, 88, 388
Chon G., Bohringer H., Nowak N., 2013, MNRAS, 429, 3272
Ciliegi P., Zamorani G., Hasinger G., Lehmann I., Szokoly G., Wilson G., 2003, A&A, 398, 901
Cohen A. S., Lane W. M., Cotton W. D., Kassim N. E., Lazio T. J. W., Perley R. A., Condon J. J., Erickson W. C., 2007, AJ, 134, 1245
Colla G. et al., 1970, A&AS, 1, 281
Colla G. et al., 1972, A&AS, 7, 1
Colla G. et al., 1973, A&AS, 11, 291
Condon J. J., Cotton W. D., Greisen E. W., Yin Q. F., Perley R. A., Taylor G. B., Broderick J. J., 1998, AJ, 115, 1693
Cutri R. M. et al., 2013, VizieR Online Data Catalog: II/328
Dalton G. B., Maddox S. J., Sutherland W. J., Efstathiou G., 1997, MNRAS, 289, 263
de Ruiter H. R., Willis A. G., Arp H. C., 1977, A&A, 28, 211
Dehghan S., Johnston-Hollitt M., Franzen T. M. O., Norris R. P., Miller N. A., 2014, AJ, 148, 75
Donoso E., Best P. N., Kauffmann G., 2009, MNRAS, 392, 617
Douglass E. M., Blanton E. L., Clarke T. E., Randall S. W., Wing J. D., 2011, ApJ, 743, 199
Ebeling H., Mullis Christopher R., Tully R. B., 2002, ApJ, 580, 774
Eilek J. A., Owen F. N., 2002, ApJ, 567, 202
Eilek J. A., Burns J. O., O'Dea C. P., Owen F. N., 1984, ApJ, 278, 37
Eke V. R., 2004, MNRAS, 348, 866
Fanaroff B. L., Riley J. M., 1974, MNRAS, 167, 31
Feretti L., Giovannini G., Klein U., Mack K. -H., Sijbring L. G., Zech G., 1998, A&A, 331, 475
Feretti L., Dallacasa D., Govoni F., Giovannini G., Taylor G. B., Klein U., 1999, A&A, 344, 472
Ficarra A., Grueff G., Tomassetti G., 1985, A&A, 59, 255
Gal R. R., Lopes P. A. A., de Carvalho R. R., Kohl-Moreira J. L., Capelato H. V., Djorgovski S. G., 2009, AJ, 137, 2981
Gan Z., Li H., Li S., Yuan F., 2017, APJ, 839, 14
Giacintucci S., Venturi A, 2009, A&A, 505, 55
Gottlöber S., Yepes G., Khalatyan A., Sevilla R., Turchaninov V., 2006, in Manoz C., Yepes G., eds, AIP Conf. Proc. Vol. 878, The Dark Side of the Universe. Am. Inst. Phys., New York, p. 3
Gower J. F. R., Scott P. F., Wills D., 1967, MNRAS, 71, 49
Gregory P. C., Condon J. J., 1991, ApJS, 75, 1011
Griffith M. R., Wright A. E., Burke B. F., Ekers R. D., 1994, ApJS, 90, 179
Gunn J. E. et al., 2006, AJ, 131, 2332
Hales S. E. G., Baldwin J. E., Warner P. J., 1988, MNRAS, 234, 919
Hales S. E. G., Masson C. R., Warner P. J., Baldwin J. E., 1990, MNRAS, 246, 256
Hales S. E. G., Baldwin J. E., Warner P. J., 1993a, MNRAS, 263, 25
Hales S. E. G., Masson C. R., Warner P. J., Baldwin J. E., Green D. A., 1993b, MNRAS, 262, 1057
Hales S. E. G., Mayer C. J., Warner P. J., Baldwin J. E., 1991, MNRAS, 251, 46
Hao J. et al., 2010, ApJS, 191, 254
Hardcastle M. J., Worrall D. M., Kraft R. P., Forman W. R., Jones C., Murray S. S., 2003, ApJ, 593, 169
Hardcastle M. J., Sakelliou I., Worrall D. M., 2005, MNRAS, 359, 1007
Healey S. E. et al., 2007, ApJS, 171, 61
Hill G. J., Lilly S. J., 1991, ApJ, 367, 1
Huchra J. P., Vogeley M. S., Geller M. J., 1999, ApJS, 121, 287
Intema H. T., Jagannathan P., Mooley K. P., Frail D. A., 2017, A&A, 598, A78
Ishwara-Chandra C. H., Sirothia S. K., Wadadekar Y., Pal S., Windhorst R., 2010, MNRAS, 405, 436
Jarrett T. H., Chester J., Cutri R., Schneider S., Skrutskie M., Huchra J. P., 2000, AJ, 119, 2498
Jones T. W., Owen F. N., 1979, ApJ, 234, 818
Kapahi V. K., Athreya R. M., van Breugel W., McCarthy P. J., Subrahmanya C. R.,1998, ApJS, 118, 275
Khatri R., 2016, A&A, 592, 48
Koester B. P. et al., 2007, ApJ, 660, 239
Kollgaard R. I., Brinkmann W., Chester M. M., Feigelson E. D., Hertz P., Reich P., Wielebinski R., 1994, ApJS, 93, 145
Large M. I., Mills B. Y., Little A. G., Crawford D. F., Sutton J. M., 1981, MNRAS, 194, 693L
Leahy J. P., Williams A. G., 1984, MNRAS, 210, 929
Lopes P. A. A., de Carvalho R. R., Gal R. R., Djorgovski S. G., Odewahn S. C., Mahabal A. A., Brunner R. J., 2004, AJ, 128, 1017

Lumsden S. L., Nichol R. C., Collins C. A., Guzzo L., 1992, MNRAS, 258, 1
Mahony E. K. et al., 2016, MNRAS, 463, 2997
Malmquist K. G., 1922, Lund Medd. Ser. I, 100, 1
Malmquist K. G., 1936, Stockholms Obs. Medd., 12, 7
Mao M. Y., Sharp R., Saikia D. J., Norris R. P., Hollitt M. J., Middelberg E., Lovell J. E. J., 2010, MNRAS, 406, 2578
Mauch T., Murphy T., Buttery H. J., Curran J., Hunstead R. W., Piestrzynski B., Robertson J. G., Sadler E. M., 2003, MNRAS, 342, 1117
McGilchrist M. M., Baldwin J. E., Riley J. M., Titterington D. J., Waldram E. M., Warner P. J., 1990, MNRAS, 246, 110
McGlynn T. A. et al., 2004, ApJ, 616, 1284
Mguda Z., Faltenbacher A., van der Heyden K., Gottlöber S., Cress C., Vaisanen P., Yepes G., 2015, MNRAS, 446, 3310
Miley G. K., Perola G. C., van der Kruit P. C., van der Laan H., 1972, Nature, 237, 269
Miller C. J. et al., 2005, AJ, 130, 968
Missaglia V., Massaro F., Capetti A., Paolillo M., Kraft R. P., Baldi R. D, Paggi A., 2019, A&A, 626, A8
Moore B., Frenk C. S., White S. D. M., 1993, MNRAS, 261, 827
O'Brien A. N., Norris R. P., Tothill N. F. H., Filipović M. D., 2018, MNRAS, 481, 4
O'Dea C. P., Owen F. N., 1985, AJ, 90, 927
O'Dea C. P., Owen F. N., 1986, ApJ, 301, 841
O'Donghue A. A., Owen F., Eilek J. A., 1990, ApJS, 72, 75
O'Donoghue A. A., Eilek J. A., Owen F. N., 1993, ApJ, 408, 428
Owen F. N., Rudnick L, 1976, ApJ, 205, L1
Owen F., Burns J., Rudnick L., 1978, ApJ, 226, LI19
Pal S., Kumari S., 2022, preprint (arXiv:2103.15153)
Patra D., Pal S., Konar C., Chakrabarti S. K., 2019, Ap&SS, 364, 72
Piffaretti R., Arnaud M., Pratt G. W., Pointecouteau E., Melin J. B., 2011, A&A, 534, 109
Pilkington J. D. H., Scott J. F., 1965, MNRAS, 69, 183
Pinkney J., Burns J. O., Rhee G., Hill J. M., 1992, BAAS, 24, 193
Pinkney J., Burns J. O., Rhee G., Hill J. M., 1998, AJ, 108, 2031
Prestage R. M., Peacock J. A., 1988, MNRAS, 230, 131
Proctor D. D., 2011, ApJS, 194, 31
Proctor D. D., 2016, ApJS, 224, 18
Quintana H., Lawrie D. G., 1982, AJ, 87, 1
Randall K. E., Hopkins A. M., Norris R. P., Zinn P. -C., Middelberg E., Mao M. Y., Sharp R. G., 2012, MNRAS, 421, 1644
Richter G. A., 1975, Astron. Nachr., 296, 65
Rozo E., Rykoff E. S., Becker M., Reddick R. M., Wechsler R. H., 2015, MNRAS, 453, 38
Sasmal T. K., Bera S., Pal S., Mondal S., 2022, ApJS, 259, 31
Sebastian B., Lal D. V., Rao A., 2017, AJ, 154, 169
Shimwell T. W. et al., 2019, A&A, 622, A1
Skrutskie M. F. et al., 2006, AJ, 131, 1163
Smith A. G., Hopkins A. M., Hunstead R. W., Pimbblet K. A., 2012, MNRAS, 422, 25
Smith D. J. B. et al., 2011, MNRAS, 416, 857
Smolcic V. et al., 2007, ApJS, 172, 295
Srivastava S., Singhal A. K., 2020, MNRAS, 493, 3811
Stocke J., 1977, PhD thesis, Univ. Arizona
Sun M., Jerius D., Jones C., 2005, AJ, 633, 165
Sutherland W., Saunders W., 1992, MNRAS, 259, 413
Swarup G. et al., 1991, Current Sci., 60, 95
Tasse C., Best P. N., Röttgering H., Le Borgne D., 2008, A&A, 490, 893
Terni de Gregory B. et al., 2017, A&A, 608, A58
Vallee J. P., Bridle A. H., Wilson A. S., 1981, ApJ, 250, 66
Van Velzen S., Falcke H., Körding E., 2015, MNRAS, 446, 2985
Vessey S. J., Green D. A., 1998, MNRAS, 294, 607
Waldram E. M., Yates J. A., Riley J. M., Warner P. J., 1996, MNRAS, 282, 779
Wen Z. L., Han J. L., 2015, ApJ, 807, 178
Wen Z. L., Han J. L., Liu F. S., 2012, ApJS, 199, 34
Wetzel A. R., Tinker J. L., Conroy C., 2012, MNRAS, 424, 232
White R. A., Bliton M., Bhavsar S. P., Bornmann P., Burns J. O., Ledlow M. J., Loken C., 1999, AJ, 118, 2014
Wing J. D., Blanton E. I., 2011, AJ, 141, 88
Worrall D. M., Birkinshaw M., 2000, ApJ, 530, 719
Wright E. L. et al., 2010, AJ, 140, 1868
Xu C., O'dea C. P., Biretta J. A., 1999, AJ, 117, 2626
Yoon J. H., Schawinski K., Sheen Y.-K., Ree C. H., Yi S. K., 2008, ApJS, 176, 414
Yu-Xing L., Hai-Guang X., Dong-Chao Z., Wei-Tian L., Zheng-Hao Z., Zhi-Xian M., Xiao-Li L., 2019, Res. Astron. Astrophys., 19, 127
Zwicky F., Herzog E., Wild P., Karpowicz M., Kowal C. T., 1961, Pasadena: California Institute of Technology (CIT), 1

SUPPORTING INFORMATION

Supplementary data are available at *MNRAS* online.

Figure-NAT.zip
Figure-WAT.zip

Please note: Oxford University Press is not responsible for the content or functionality of any supporting materials supplied by the authors. Any queries (other than missing material) should be directed to the corresponding author for the article.

This paper has been typeset from a TEX/LATEX file prepared by the author.